The impact of stratospheric model configuration on planetary scale waves in northern hemisphere winter

Tiffany A. Shaw *

Center for Atmosphere Ocean Science, Courant Institute of Mathematical Sciences,

New York University, New York, New York, USA

Judith Perlwitz

Cooperative Institute for Research in Environmental Sciences, University of Colorado/NOAA

Earth System Research Laboratory, Boulder, CO, USA.

Submitted 17 September 2009, Revised 01 February 2010

* *Corresponding author address:* Dr. Tiffany A. Shaw, Center for Atmosphere Ocean Science, Courant Institute of Mathematical Sciences, New York University, 251 Mercer St., New York, NY 10012.

E-mail: tshaw@cims.nyu.edu

ABSTRACT

The impact of stratospheric model configuration on modeled planetary scale waves in northern hemisphere winter is examined using the Canadian Middle Atmosphere Model. The CMAM configurations include a high-lid (0.001 hPa) and a low-lid (10 hPa) configuration which were each run with and without conservation of parameterized gravity wave momentum flux.

The planetary wave structure, vertical propagation and the basic state are found to be in good agreement with reanalysis data for the high-lid conservative configuration with the exception of the downward propagating wave one signal. When the lid is lowered and momentum is conserved, the wave characteristics and basic state are not significantly altered, with the exception of the downward propagating wave one signal, which is damped by the act of conservation. However when momentum is not conserved the wave amplitude increases significantly near the lid, there is a large increase in both the upward and downward propagating wave one signals and a significant increase in the strength of the basic state. The impact of conserving parameterized gravity wave momentum flux is found to be much larger than that of the model lid height.

The changes to the planetary waves and basic state significantly impact the stratosphere-troposphere coupling in the different configurations. In the low-lid configuration there is an increase in wave reflection type coupling over zonal-mean type coupling, a reduction in stratospheric sudden warming events and an increase in the Northern Annular Mode time scale. Conserving gravity wave momentum flux in the low-lid configuration significantly reduces these biases.

1. Introduction

Planetary scale waves play an important role in determining the climate of the winter hemisphere. They are a particularly important component of the dynamics of the winter season in the northern hemisphere where they are readily forced by the combination of orography and continent-ocean heating asymmetries. Planetary waves are well known to be one of the dominant modes of coupling between the stratosphere and troposphere due to their significant vertical propagation. They induce both zonal-mean and wave reflection type coupling. In the case of zonal-mean coupling, wave-mean flow interactions in the stratosphere in northern hemisphere winter induce zonal-mean anomalies which have been shown to have non-negligible effects on surface climate on intraseasonal time scales (Baldwin and Dunkerton 2001). In the case of wave reflection type coupling, the waves are reflected back into the troposphere and these events dominate the coupling on short time scales (up to 12 days) (Perlwitz and Harnik 2003, 2004). A proper representation of the structure and propagation characteristics of planetary waves is required for the accurate modeling of the stratosphere-troposphere coupled system as well as for the climate system as a whole.

Here we examine the impact of stratospheric model configuration on planetary waves in northern hemisphere winter. We focus on two aspects of the configuration: the model lid height and conservation of parameterized gravity wave drag (GWD) momentum flux. GWD parameterizes the unresolved transfer of momentum by gravity waves, which must be included in climate models for an accurate simulation of both upper tropospheric winds and Antarctic stratospheric temperatures (McFarlane 1987; Garcia and Boville 1994). It is well known that parameterized GWD strongly interacts with planetary waves through the mean

flow during northern hemisphere winter (McLandress and McFarlane 1993).

Previous authors have investigated the impact of stratospheric jet strength and model lid height on tropospheric climate and noted a large impact of both on planetary wave structure. Boville (1984) considered the impact of stratospheric jet strength on planetary waves in the troposphere in two-year perpetual January model simulations. They noted a large difference in planetary wave one amplitude and phase at 500 hPa for weak versus strong jet states. The differences in the jet resulted in large changes in the blocking frequency in the Euro-Atlantic sector. In particular, when the jet was strong there were very few blocking events. Using a similar model set-up, Boville (1986) considered the differences in wave-mean flow interaction in weak versus strong jet states and noted a feedback whereby a strong stratospheric jet favors weak planetary wave forcing while the opposite is true for a weak jet. Finally, Boville and Cheng (1988) performed two-year perpetual January model lid height sensitivity simulations using two lid height configurations: 10 and 0.5 hPa. They noted a large impact on planetary wave amplitude and phase throughout the depth of the atmosphere when they lowered the model lid. In particular the wave amplitude was very large in the vicinity of the model lid and the phase lines were tilted in the vertical. They argued that these changes were indications of increased wave reflection in the low-lid model. While Boville and Cheng (1988) considered the impact of lid height on the structural aspects of the waves they did not consider the impact on the propagation characteristics of the waves. In particular they did not confirm the increase in the downward propagating (reflective) signal. Furthermore, none of the previous authors considered the impact of conservation of gravity wave momentum flux on planetary wave structure and propagation. (The models used by the previous authors did not include any parameterized GWD.)

The impact of conservation of parameterized gravity wave momentum flux on modeled climate was only noted recently by Shaw et al. (2009). Shaw et al. (2009) ran the Canadian Middle Atmosphere Model in two model lid height configurations (10 hPa and 0.001 hPa) with and without conservation of gravity wave momentum flux and found that both factors affected the tropospheric climate, in both hemispheres, with conservation having the larger impact. They noted that the large impact of momentum conservation in the low-lid configuration was the result of changes in planetary wave drag induced downwelling. However, they did not investigate the cause of the changes, in particular how the wave structure and propagation were being affected by the low-lid and by momentum conservation.

A clear identification of the impacts of the stratospheric model configuration on planetary waves requires diagnostics of both the planetary wave structure and vertical propagation. Perlwitz and Harnik (2003) used a singular value decomposition analysis to isolate the vertical propagation characteristics (both upward and downward) of observed planetary waves. Here we use their analysis to understand the effects of stratospheric model configuration on the propagation characteristics of modeled planetary waves. We compare the models with reanalysis data for completeness. We also investigate the implications of the impacts on the planetary waves on the coupling between the stratosphere and troposphere. Without the proper coupling the impact of the stratosphere on tropospheric climate and climate change, which is an important topic of current research (Shaw and Shepherd 2008), cannot be properly assessed.

Section 2 describes the model and reanalysis data sets used in this study. Section 3 discusses the impact of stratospheric model configuration on planetary wave structure while section 4 focuses on the impact on planetary wave propagation. In section 5 the impact on

the coupling between the stratosphere and troposphere is investigated. The paper concludes with a summary and discussion in section 6.

2. Model and reanalysis data

The model data used in this study is from a series of Canadian Middle Atmosphere Model (CMAM) model experiments performed by Shaw et al. (2009), hereafter S09. The CMAM version used by S09 is the same as that used for the 2006 World Meteorological Organization Ozone Assessment (Eyring et al. 2006), except that the interactive chemistry is turned off. In S09, the CMAM was run in two different lid height configurations with and without conservation of gravity wave momentum flux. The first model lid height was the standard configuration with 71 vertical levels from the surface up to 0.001 hPa ($\sim$ 100 km), labeled HIGH, and the second configuration was a low-lid configuration with 41 vertical levels and the model lid slightly above 10 hPa, labeled LOW (Sigmond et al. 2008). The two lid-height configurations have identical vertical resolution and parameterization settings. Each lid-height configuration was run for 40 years with and without conservation of gravity wave momentum flux as described by S09. Conservation of gravity wave momentum flux was enforced by depositing any gravity wave momentum flux at the model lid in the uppermost model level (see section 2 of S09 for details). As in S09 we will refer to gravity wave momentum flux conservation as momentum conservation. The high-lid conservative configuration is labeled HIGH_C. Because there was little impact of conservation on the high-lid model, as discussed by S09, in what follows we will not discuss the high-lid non-conservative configuration. The low-lid conservative and non-conservative configurations are

labeled LOW_C and LOW_N, respectively. The reanalysis data set used in this study is the four-times-daily reanalysis of the National Center for Environmental Prediction-National Center for Atmospheric Research from January 1979 to March 2009 (NCEP-NCAR; Kalnay et al. 1996).

Here we focus on high winter (January, February and March, JFM) in the northern hemisphere since it is during this time that planetary waves interact most strongly with the mean flow. In particular, during JFM there are the largest number of observed stratospheric sudden warming events (Charlton and Polvani 2007) and the largest number of planetary wave reflection events (Perlwitz and Harnik 2003). Finally, it was during JFM that the largest differences in polar cap averaged temperature and planetary wave drag induced downwelling were reported between the different CMAM configurations (see S09 Figs. 1 and 4).

3. Impact on planetary wave structure

We begin our analysis of planetary wave structure with the impact of stratospheric model configuration on the stratospheric basic state since it is well known that the basic state mediates the transmission and reflective properties of the waves into the upper atmosphere (Charney and Drazin 1961; Matsuno 1970). Figure 1 shows the zonal-mean zonal wind in JFM for the reanalysis and the different CMAM configurations. Regions where the zonal-mean zonal winds exceed 15 ms^{-1} are shaded. The corresponding stratospheric jet variability is shown in Fig 2. In Fig. 2 the solid lines are the averaged zonal-mean zonal wind between 58 and 74°N while the dashed lines are composites of the years which exceed $\pm$ 0.5 standard deviations of the average at 30 hPa. A similar characterization of jet variability was used by

Perlwitz and Harnik (2003) (see their Fig. 14a).

The reanalysis data shows a strong stratospheric jet which peaks in the upper stratosphere (Fig. 1 top left) and exhibits clear weak and strong states (Fig. 2 top left). In the weak-jet state there is weak vertical shear below 10 hPa whereas in the strong-jet state there is strong vertical shear. The HIGH_C stratospheric jet in JFM (Fig. 1 top right) is slightly weaker than in the reanalysis and has a wider region of connection between the stratospheric and tropospheric jets. The jet variability is in good agreement with the reanalysis (Fig. 2 top right). When the model lid is lowered and momentum is conserved, the jet strengthens such that it becomes stronger than in the reanalysis (Fig. 1 bottom left). However the difference between the HIGH_C and LOW_C jets is less than 5 ms^{-1} throughout most of the domain. The corresponding change in jet variability is also minimal (Fig. 2 bottom left). A much larger change in the jet occurs when momentum is not conserved in the low-lid model. In particular, the jet strength increases by a factor of three (Fig. 1 bottom right) and there is no longer a weak-jet state (Fig. 2 bottom right). The jet always has strong vertical shear below 10 hPa. These changes in the jet coincide with changes in zonal-mean temperature and lead to a significant cold bias in LOW_N as noted by S09 (see their Fig. 2). They are also expected to cause changes in the planetary wave structure and propagation. It is clear that both model lid height and conservation of momentum impact the stratospheric jet with nonconservation having the largest impact.

Figure 3 shows the longitudinal structure of the JFM geopotential height field at 500 hPa in HIGH_C and the difference with the other CMAM configurations. The 500 hPa height field in HIGH_C is in reasonable agreement with the reanalysis (not shown). When the lid is lowered and momentum is conserved, there is very little impact on the height field at

500 hPa. The difference between HIGH_C and LOW_C shows only a very small region of statistical significance (Fig. 3 top right). When the lid is lowered and momentum is not conserved, there is a much larger and more statistically significant impact on the height field at 500 hPa (Fig. 3 bottom left). The difference between LOW_N and HIGH_C is very similar to the difference between LOW_N and LOW_C suggesting that it is conservation and not the lid height which has the largest impact on the height field at 500 hPa.

The impact on the wave field at 500 hPa is consistent with the results of previous authors. Boville (1984) found that the strength of the stratospheric jet significantly impacted the 500 hPa height field. In particular there was a marked ridging in the eastern Atlantic and on the west coast of North America indicative of blocking when the stratospheric jet was weak which was not present when the jet was strong (see their Fig. 3). The pattern is similar to the differences between LOW_N and HIGH_C and between LOW_N and LOW_C. Boville and Cheng (1988) found a similar impact on the height field at 500 hPa when they lowered their model lid from 0.5 to 10 hPa (see their Fig. 7). The lowering of the lid coincided with an increase in strength of the stratospheric jet which was argued to be the cause of the changes in the height field. However here it is shown that lowering the model lid does not lead to large changes in either the zonal-mean winds or the height field at 500 hPa so long as momentum is conserved.

Figure 4 shows the JFM blocking frequency as a function of longitude for the reanalysis and the CMAM configurations. The blocking frequency is calculated following Tibaldi and Molteni (1990).[1] The HIGH_C blocking frequency (dashed line) shows a bias in the location

[1]See page 345 of Tibaldi and Molteni (1990). For the reanalysis data we set ϕ_n=80°N, ϕ_0=60°N, ϕ_s=40°N and Δ=-5°, 0°, 5° and for the CMAM data we set ϕ_n=79.5°N, ϕ_0=60.0°N, ϕ_s=40.5°N and Δ=-5.6°, 0°,

of blocking in the Euro-Atlantic sector as compared to the reanalysis (solid line). There are also too few blocking events which is a common model bias (see D'Andrea and coauthors (1998) Fig 4). When the lid is lowered and momentum is conserved there is very little impact on the blocking frequency (dash-dot line) with the exception of a decrease in the region between 30-90°W which coincides with the largest differences in the geopotential height at 500 hPa between LOW_C and HIGH_C (see Fig. 3 top right). When the lid is lowered and momentum is not conserved, there is a much larger impact on the frequency. In particular, between 0-90°W there is a significant decrease in the frequency and between 0-180°E there is an increase both of which are consistent with the differences in the geopotential height at 500 hPa between LOW_N and HIGH_C (see Fig. 3 bottom left). As mentioned above, Boville and Cheng (1988) noted a significant decrease in the blocking frequency in the Euro-Atlantic sector between their high and low lid models. Here it is shown that lowering the model lid does not lead to significant changes in the blocking frequency so long as momentum is conserved.

The differences in the height field at 500 hPa between the CMAM configurations are dominated by differences in the planetary wave one contribution. Figure 5 shows the wave one pattern at 500 hPa in the reanalysis and the different CMAM configurations. The HIGH_C wave one pattern is in fairly good agreement with the reanalysis (compare Fig. 5 top right with top left). The amplitude is slightly too weak and there is a slight difference in phase. When the model lid is lowered and momentum is conserved the wave one pattern is not significantly altered (Fig. 5 bottom left). When momentum is not conserved however there is a distortion of the wave one pattern over the polar cap with the amplitude increasing

5.6°.

by a factor of two (Fig. 5 bottom right). There is much more horizontal tilt to the wave axis and this results in the large amplitude at high latitudes. A similar change in wave one over the polar cap was found by Boville (1984) and coincided with a strengthening of the stratospheric jet. Note that the changes in the wave one pattern in LOW_N also coincide with a strengthening of the jet. The large wave one amplitude in high-latitudes in LOW_N is also reminiscent of the downward propagating wave reflection pattern at 500 hPa isolated by Perlwitz and Harnik (2003) (see their Fig. 3b). They identified the pattern with wave reflection since it was associated with an eastward phase tilt with height. Momentum conservation clearly leads to a more realistic wave one pattern over the polar cap. This effect of conservation was not considered in previous studies.

The changes in phase and amplitude of wave one at 500 hPa coincide with large changes in amplitude at higher altitudes. Figure 6 shows the zonal-mean wave one amplitude as a function of latitude in the reanalysis and the different CMAM configurations. The reanalysis show a clear increase of the planetary wave one amplitude in the stratosphere (Fig. 6 top left). The phase lines also tilt westward with height and northeast-southwest with latitude indicative of upward and poleward energy flux (not shown). The HIGH_C wave one structure is in good agreement with the reanalysis both in terms of its amplitude (Fig. 6 top right) and its phase (not shown). When the lid is lowered and momentum is conserved, the wave amplitude is not significantly altered (Fig. 6 bottom left). When momentum is not conserved, there is a very large increase in amplitude near the model lid (Fig. 6 bottom right). Both the wave one amplitude and phase in LOW_N show strong indications of wave reflection. In particular, there is both a large increase in amplitude and a pronounced vertical tilt in the phase lines (not shown) near the lid. It is clear that momentum conservation

significantly impacts the structure of wave one in the low-lid model.

As discussed previously, Boville and Cheng (1988) conjectured that planetary wave one in their low lid (10 hPa) model was undergoing significant reflection based on a large increase in wave amplitude and vertically tilted phase lines near the model lid. Sassi et al. (2010) also noted vertically tilted phase lines in the low-lid version of the NCAR model (the Community Atmospheric Model) which did not occur in the high-lid version (the Whole Atmosphere Community Climate Model) and also argued based on those diagnostics that there was more wave reflection in the low-lid model. (Note that the two NCAR model versions do not have the same vertical resolution or parameterization settings and thus the comparison is not as clean as for the CMAM configurations. Furthermore, the authors did not discuss whether or not the models were conservative.) However, the previous authors did not confirm an increase of wave reflection via model diagnostics of wave one propagation. Furthermore they did not assess whether the upward propagating wave was also being affected. It is important to note that the height field at any level is a combination of upward and downward propagating contributions and that monthly, zonal-mean diagnostics cannot isolate the space-time structure of the wave one field.

4. Impact on vertical propagation characteristics

To assess the impact of stratospheric model configuration on the propagation of planetary wave one we apply the time-lagged singular value decomposition (SVD) analysis of Perlwitz and Harnik (2003), hereafter PH03. PH03 applied the SVD analysis to NCEP data for 90-day seasonal periods from 1979/80 to 2001/02 to isolate upward and downward propagating

wave one patterns. The upward and downward propagating patterns are sufficiently different because they correspond to westward and eastward phase tilts with height associated with upward and downward energy flux, respectively. (Note that the SVD analysis cannot distinguish cases of wave refraction in latitude.) Using the SVD analysis, PH03 showed clear evidence of planetary wave one reflection in the reanalysis. We refer the reader to PH03 for a detailed description of the analysis procedure.

Figure 7 shows correlation coefficients of the time-dependent expansion coefficient for the leading coupled SVD mode between wave one geopotential data at 500 hPa and data at three different stratospheric levels (50 hPa dash-dot, 30 hPa solid and 10 hPa dashed), as a function of time lag for the reanalysis data and the different CMAM configurations. The stratospheric field is held fixed and thus negative lags have the troposphere leading the stratosphere and positive lags have the stratosphere leading the troposphere. The correlation coefficients for the reanalysis, shows two distinct maxima; one maximum for both negative and positive lags (Fig. 7 top left panel). The results differ slightly from those in Fig. 2 of PH03 because 7 more years of reanalysis data have been included. The correlation maxima are well above the threshold of statistical significance which is 0.1 at the 95% level. (The statistical significance is calculated by taking into account the autocorrelations of the time series (Lau and Chan 1983)). For negative lags, the maxima occur at -6, -5, -4 day lags for the 10, 30, and 50 hPa levels consistent with an upward propagating wave signal. According to the SVD analysis, it takes planetary wave one approximately 2 days to propagate upwards from 50 hPa to 10 hPa. The associated spatial patterns show a clear westward phase tilt with height (Table 1 top left panel), which indicates upward energy flux. For positive lags, the maximum correlations occur at +5, +6, and +7 day lags for the different levels. It takes

approximately 2 days for the wave pattern to propagate back downwards from 10hPa to 50 hPa. The associated spatial pattern shows a clear eastward phase tilt with height (Table 1 top left panel) which indicates downward energy flux.

The correlation coefficients in HIGH_C also show two distinct, statistically significant, correlation maxima (Fig. 7 top right panel). (The 95% statistically significant level for all the CMAM configurations is approximately 0.08.) For negative lags, the maximum correlation coefficients at the three stratospheric levels are in fairly good agreement with the reanalysis. The upward propagation of the wave one pattern from 50 to 10 hPa takes slightly less than two days in HIGH_C. There is also a clear westward phase tilt with height for the corresponding spatial patterns (Table 1 top right panel). For positive lags, the correlations are much weaker than those in the reanalysis. Furthermore, the separation between the different stratospheric levels is not statistically significant and thus a downward propagation time scale cannot be estimated. However, there is a clear eastward phase tilt with height in the corresponding spatial patterns (Table 1 top right panel). While HIGH_C is able to model the upward propagation it does not accurately represent the observed reflection of planetary wave one. When the lid is lowered and momentum is conserved, the correlation coefficients and propagation time scale remain in good agreement with the reanalysis for negative lags (Fig. 7 bottom left panel). The corresponding spatial patterns and their westward phase tilt with height is also preserved (Table 1 bottom left panel). For positive lags, the correlations remain similar to those for HIGH_C and once again a time scale for downward propagation cannot be discerned. There is a suggestion that the downward propagating signal may be damped as there is virtually no separation between the correlation maxima for the different stratospheric levels. However, the eastward phase tilt with height is preserved (Table 1

bottom left panel). When the lid is lowered and momentum is not conserved, there are very large changes to the propagation characteristics (Fig. 7 bottom right panel). For negative lags, the maximum correlations are much larger than both the reanalysis and the other two CMAM configurations. The time scale of upward propagation decreases to 1 day. (The switch in the order of the maxima of the curves is not statistically significant.) However, the westward phase tilt with height is preserved (Table 1 bottom right panel). For positive lags, the correlations also increase significantly. The downward propagation time scale is less than 1 day. Once again the eastward phase tilt with height is preserved (Table 1 bottom right panel). The SVD analysis suggests that there is significantly more downward propagation of planetary wave one (wave reflection) in LOW_N than in the other configurations, which is consistent with the analysis in the previous section.

The histogram of the correlation coefficients at 30 hPa for +6 day lag for all years is shown in Fig. 8. The reanalysis show a distribution of correlation coefficients with a mean which is above the threshold of statistical significance (Fig. 8 top left). In HIGH_C the mean of the distribution is less than in the reanalysis (Fig. 8 top right). In particular, a larger fraction of the years have correlation coefficients closer to the threshold of statistical significance, which is consistent with the correlation maximum for positive lags in HIGH_C being weaker than in the reanalysis (see Fig. 7 top right versus top left). When the lid is lowered and momentum is conserved, the distribution is preserved (Fig. 8 bottom left). There is no statistically significant change in the mean or variance. When momentum is not conserved, there are much larger changes to the distribution (Fig. 8 bottom right). The LOW_N distribution has a mean which is twice as large as that of HIGH_C. This is consistent with the large correlations found for positive lags (Fig. 7 bottom right).

The significant changes in the wave one vertical propagation characteristics in the low-lid configurations are due primarily to changes in wave reflection. PH03 showed that the correlation maximum for positive lags in the reanalysis was strongly correlated with the jet structure. They defined a jet index based on the difference between the zonal wind at 2 and 10 hPa, U(2-10hPa), with the zonal wind averaged between 58 and 74°N. Negative (positive) index states were defined when the difference was less (more) than 0.5 of the standard deviation. The correlation maximum for positive lags was shown to be largest for months when the jet was in a negative index state with negative shear in the upper stratosphere. The negative shear was responsible for creating a reflecting surface, which caused the increase in the correlation for positive lags. Given that the model lid in LOW_C and LOW_N is at 10 hPa, a reflecting surface never develops as it does in the real atmosphere, however the model lid acts as a permanent reflecting surface. The strong positive shear below 10 hPa in LOW_N likely acts as a wave guide towards the lid leading to more wave reflection there and hence the large increase in the correlation maximum for positive lags. The differences between the LOW_N and LOW_C jets and consequently the amount of wave reflection must be related to conservation of momentum. This is examined further below. In HIGH_C the lid is well above the 2 hPa level and thus the wave reflection is caused by a reflecting surface and not by the model lid. However, when the PH03 index is calculated for the HIGH_C configuration the index is rarely negative suggesting that the basic state rarely develops a reflecting surface and this causes the disagreement with the reanalysis for positive lags.

We can further confirm the changes in wave reflection in the different CMAM configurations by looking at histograms of the daily heat flux in JFM. The heat flux is the dominant contributor to the vertical component of the Eliassen-Palm flux (Andrews et al. 1987). New-

man et al. (2001) showed that the heat flux during January and February is highly correlated with polar cap averaged temperatures in February and March. S09 calculated the Newman-type diagnostic for the different CMAM configurations (see their Fig. 3) and it was clear from the monthly averaged data that there were fewer large heat flux values in the LOW_N configuration, which lead to much colder temperatures. However, to discern whether there are strictly negative values, indicating downward propagation, daily data is required. A histogram of daily wave one heat flux values averaged between 40 and 90°N at 100 hPa in JFM for the reanalysis and the different CMAM configurations is shown in Fig. 9. The reanalysis and HIGH_C are in excellent agreement (Fig. 9 top two panels). The fraction of days where the averaged wave one heat flux is negative, indicating a day with more downward propagation than upward propagation through 100 hPa, are very similar. When the lid is lowered and momentum is conserved, the distribution is not significantly altered (Fig. 9 bottom left). However, when momentum is not conserved the fraction of days with negative wave one heat flux values increases dramatically (by a factor of 2) and the mean is reduced (Fig. 9 bottom right). This further confirms that there are a large number of reflection events in LOW_N, which penetrate all the way down to 100 hPa and is consistent with the changes in tropospheric wave one structure (Fig. 3 bottom right panel).

Figure 10 shows the corresponding wave one heat flux histogram at 10 hPa. Once again the reanalysis and HIGH_C are in excellent agreement (Fig. 10 top two panels). The distribution at this level is clearly skewed. When the lid is lowered and momentum is conserved, the standard deviation of the distribution is significantly reduced (Fig. 10 bottom left). There are fewer large positive wave one heat flux values. This suggests that the low-lid model in combination with momentum conservation is damping wave one near the

model lid and is consistent with the lack of separation between the correlation values for the different stratospheric levels in the SVD analysis for positive lags (Fig. 7 bottom left). When momentum is not conserved, the fraction of days with negative wave one heat flux values increases by a factor of 4 and the number of large positive wave one heat flux values also increases. This suggests that more wave one heat flux is reaching the lid in LOW_N and consequently being reflected there. This is in contrast with the case when momentum is conserved where conservation appears to directly damp wave one near the lid thereby reducing the amount of spurious lid reflection.

The damping of wave one near the model lid in LOW_C can be confirmed by looking at the structure of the GWD near the lid. Figure 11 shows the wave one pattern of the GWD (orographic and nonorographic) at 10 hPa and the corresponding wave one pattern of the zonal wind. In all model configurations the GWD at 10 hPa is dominated by the orographic component as discussed by S09. The HIGH_C configuration shows a significant wave one projection of the GWD at 10 hPa (Fig. 11 top left). The wave one GWD is out of phase with the wave one zonal wind suggesting that it is damping wave one at 10 hPa (Fig. 11 top right). When the lid is lowered and momentum is conserved, the wave one projection of the GWD increases by a factor of two, particularly towards the pole (Fig. 11 middle left). As for HIGH_C, the wave one GWD is out of phase with the zonal wind and thus it is damping wave one at 10 hPa (Fig. 11 middle right), however the damping is much stronger. This is consistent with the reduction in the standard deviation of the wave one heat flux distribution at 10 hPa (Fig. 10 bottom left). In contrast, when momentum is not conserved the wave one projection of the GWD is near zero (Fig. 11 bottom left), which leads to less damping and stronger zonal winds (Fig. 11 bottom right). The lack of GWD damping in LOW_N is

consistent with the large number of positive wave one heat flux values at 10 hPa (Fig. 10 bottom right).

5. Impact on stratosphere-troposphere coupling

The of impact stratospheric model configuration on the structure and propagation characteristics of planetary waves found in the previous sections has implications for the dynamical coupling between the stratosphere and troposphere. Perlwitz and Harnik (2004), hereafter PH04, showed that the planetary wave coupling between the two regions can be separated into zonal-mean and wave reflection type coupling. In the case of zonal-mean type coupling, the planetary waves dissipate and induce zonal-mean anomalies which propagate downward on an intraseasonal time scale towards the surface (Baldwin and Dunkerton 2001). In the case of wave reflection type coupling, the planetary waves are reflected downwards into the troposphere by the stratospheric jet on a much faster time scale (less than 12 days). Both Baldwin and Dunkerton (2001) and PH04 analyzed the coupling events by calculating time-lagged correlations of the Northern Annular Mode (NAM) signature time series at 10 hPa with all other levels.

Following Baldwin and Dunkerton (2001) and PH04 we calculate time-lagged correlations of the NAM signature time series at 10 hPa with all other levels for all years. The daily unfiltered NAM time series was calculated using the zonal-mean NAM according to Baldwin and Thompson (2009) for all JFM periods. The NAM's are in good agreement in the trosposphere (not shown). In the stratosphere the NAM's are in good agreement with the exception of LOW_N which has a much larger amplitude towards to pole (not shown) and

is consistent with its stratospheric jet being much stronger than the jets in HIGH_C and LOW_C (see Fig. 2).

Figure 12 shows the correlation coefficient for the NAM signature time series at 10 hPa with all other levels for time lags between -40 and 40 days for the reanalysis and the different CMAM configurations. The reanalysis correlation shows a clear downward progression of a positive anomaly from the stratosphere which reaches the surface 10-30 days later (Fig. 12 top left). There are also large correlations values near lag zero in the stratosphere which do not extend into the troposphere and a clear vacillation of the correlation sign on an intraseasonal time scale. The results differ slightly from PH04 (see their Fig. 4a) because we have included 7 more years of reanalysis data. PH04 found that years with strong zonal-mean type coupling showed a clear downward progression of NAM anomalies towards the surface while years with strong wave reflection type coupling had no downward coupling and the correlations peaked near zero time lag. The reanalysis show features of both zonal-mean and wave reflection type coupling, as noted by PH04.

The HIGH_C configuration shows a similar downward progression of NAM anomalies and large correlation values near lag zero (Fig. 12 top right). There is however a delay in the downward progression into the troposphere: the maximum surface correlation occurs between 20-40 days. HIGH_C also captures the vacillation in the stratosphere and the phase transition from negative to positive at the surface near zero lag seen in the reanalysis. When the lid is lowered and momentum is conserved, the downward progression seen in HIGH_C is distorted (Fig. 12 bottom left). The largest correlation values occur near day zero and while there is some downward progression of the positive anomaly, it reaches the surface later than in HIGH_C (approximately 10 days later). The vacillation in the stratosphere is also weaker

and there is no longer a phase transition at the surface. The large correlation values near zero lag suggest that there is more wave reflection type coupling in LOW_C as compared to HIGH_C. The wave-mean flow interaction processes that lead to the downward progression of the zonal-mean anomalies in HIGH_C are clearly altered by the low lid in combination with momentum conservation. When momentum is not conserved there are further changes to the coupling. In particular the correlations become very large near zero lag and there is no longer any indication of a downward progression on intraseasonal time scales (Fig. 12 bottom right). The large correlation values near zero lag and lack of downward progression suggests that the coupling in LOW_N is dominated by wave reflection type coupling, which is consistent with the analysis in previous sections. It is clear that while momentum conservation improves the coupling it cannot entirely eliminate the negative effects of a low lid on the planetary waves.

The impact of the changes in the planetary waves on the stratosphere and troposphere coupling in the different CMAM configurations can be further illustrated by considering stratospheric sudden warming (SSW) events. Following Charlton and Polvani (2007) we define a SSW event as a reversal in sign of the zonal-mean zonal wind at 10 hPa and 60°N from November to March. Figure 13 shows composites of the zonal wind at 10 hPa and 60°N for SSW events in the reanalysis and the CMAM configurations. The reanalysis show a large and fast time scale decrease in the zonal-mean zonal wind preceeding the SSW event with a much slower time-scale recovery following the event (Fig. 13 top left). The reanalysis composite is based on the 18 events which occurred during the 30 year record. The SSW zonal wind composite for HIGH_C is in good agreement with the reanalysis (compare Fig. 13 top left to top right). The composite is based on the 30 events which occurred in the 40 year model run. The good agreement between the SSW events in the reanalysis and the

CMAM model in its standard high-lid configuration was highlighted recently by McLandress and Shepherd (2009). When the lid is lowered and momentum is conserved, the zonal wind composite is slightly distorted (Fig. 13 bottom left). There is a suggestion that the time scale of recovery is decreased when the lid is lowered. The composite is based on only 15 events (the number of events is reduced by half when the lid is lowered). When momentum is not conserved, the zonal wind SSW composite is completely distorted (Fig. 13 bottom right). There is a clear increase in the time scale of both the decrease in zonal wind preceding the event and its subsequent recovery. The faster time scale recovery is consistent with the lack of downward progression of NAM anomalies (Fig. 12 bottom right). There is also no decrease in the zonal wind following the event as seen in the reanalysis. It is possible that the SSW events in LOW_N involve the displacement of the stratospheric jet off of the pole rather than the destruction of the jet and its subsequent recovery. There is also a further reduction in the number of SSW events when momentum is not conserved (there are only 8 events in LOW_N). Sassi et al. (2010) also noted a distortion in the time scale and number of SSW events in their low-lid mean-sea level pressure SSW composite as compared to their high-lid composite. However they did not state whether their model was conservative or not.

Finally, the seasonal cycle of the coupling, as measured by the seasonal cycle of the NAM time scale, in the reanalysis and the different CMAM configurations is shown in Fig. 14. Using reanalysis data from 1958-2002, Baldwin et al. (2003) showed that the observed lower stratospheric and tropospheric NAM time scale maxima are coincident in the northern hemisphere during December, January and February (DJF), indicating strong stratosphere-troposphere coupling during that time. More recently, Gerber et al. (2008a) analyzed the Intergovernmental Panel on Climate Change (IPCC) AR4 models and showed that they have

large biases in the seasonal cycle of the NAM time scale in the troposphere in the northern hemisphere. The models in the IPCC AR4 are predominantly low-lid models (Cordero and Forster 2006). The observed seasonal cycle of the NAM time scale for 1979-2008 shows a maximum in the troposphere during DJF (Fig. 14 top left). The time scales are slightly different from Baldwin et al. (2003) and Gerber et al. (2008a) because we have excluded years before 1979 in the current analysis. The maximum time scale in the troposphere occurs in DJF and is approximately 13 days. The maximum time scale in the lower stratosphere also occurs in DJF and is 30 days. (The largest time scales in the stratosphere occur in summer, however the variance in the NAM during that time is minimal.) The HIGH_C configuration shows good agreement with the reanalysis in the stratosphere with a maximum time scale in the lower stratosphere in DJF of 30 days (Fig. 14 top right). The maximum time scale in the troposphere is larger than in the reanalysis and occurs in spring instead of winter. Overall, the HIGH_C time scales lie within the range of uncertainty of the reanalysis time scales with the exception of the tropospheric maximum in spring.[2] (Note that the seasonal cycle of the time scales in all the CMAM configurations are found to be robust when 20 year sub-samples are considered, however the magnitude of the time scales vary slightly.) When the lid is lowered and momentum is conserved, the maximum stratospheric time scale in winter increases slightly (Fig. 14 bottom left). In the troposphere the maximum time scale also increases and is shifted from spring to winter. Overall, LOW_C shows good agreement with the reanalysis in terms of the seasonal cycle in both the stratosphere and troposphere, however the time scales are too large in winter. In particular, the tropospheric time scale in winter is outside the range of uncertainty of the reanalysis time scale. When

[2]The uncertainty of the time scales were estimated following Gerber et al. (2008b).

momentum is not conserved the time scales are severely altered (Fig. 14 bottom right). The maximum stratospheric time scale increases by a factor of three and is more reminiscent of those observed for the southern annular mode (see Fig. 1B from Baldwin et al. (2003)). In the troposphere there are two maxima which occur in early winter and late winter/early spring, respectively. Both the tropospheric and stratospheric time scale maxima are outside the range of uncertainty of the reanalysis time scale. The increase in maximum time scale in the stratosphere in winter between LOW_C and LOW_N is consistent with the previous results: non conservation results in a very strong stratospheric jet which is more persistent and hence not easily perturbed (i.e. there are fewer SSW events). Note that the differences in time scales between the CMAM configurations likely reflect differences in the interannual variability (Keeley et al. 2009) and stratosphere-troposphere coupling is one source of this variability.

6. Summary and discussion

We have examined the impact of stratospheric model configuration on planetary wave structure, vertical propagation and the resulting impact on stratosphere-troposphere coupling in northern hemisphere winter using the CMAM. The CMAM configurations included a high-lid (0.001 hPa) and a low-lid (10 hPa) configuration which were each run with and without conservation of parameterized gravity wave momentum flux.

The impact on planetary wave structure was examined using diagnostics of the stratospheric basic state, variability, wave one horizontal structure at 500 hPa, blocking frequency and wave amplitude and phase at all vertical levels. The impact on planetary wave ver-

tical propagation (both upward and downward) was examined using the SVD analysis of PH03. The upward and downward propagating signals were isolated as maxima of time-lagged correlation coefficients of the temporal expansion coefficients of the first coupled mode between zonal wave number one geopotential data at 500 hPa and data from three different stratospheric levels (50, 30 and 10 hPa). The propagation characteristics were also investigated using histograms of the daily wave one heat flux at 100 and 10 hPa averaged between 40-90°N. Finally the impact on stratosphere-troposphere coupling was examined using time-lagged NAM correlations, SSW composites and the seasonal cycle of the NAM time scale.

The stratospheric basic state, variability and planetary wave one structure in the high-lid conservative configuration are in good agreement with reanalysis data. The blocking frequency however is biased in its position of the maximum frequency in the Euro-Atlantic sector and in its absolute frequency. The upward propagating wave one pattern and its time scale of propagation is in reasonable agreement with the reanalysis. However the high-lid conservative configuration fails to accurately capture the downward propagation of wave one: it underestimates the magnitude of the correlation and the timescale of propagation. The histogram of the daily wave one heat flux at 100 and 10 hPa in JFM are however in good agreement with the reanalysis. Both zonal-mean and wave reflection type stratosphere-troposphere coupling contribute to the time-lagged NAM correlations, which is in agreement with the reanalysis. However, the zonal-mean NAM anomalies take 15 days to reach the surface which is longer than in the reanalysis. The SSW zonal wind event composite has a reasonable time scale and subsequent recovery. Finally, the seasonal cycle of the NAM time scales in the stratosphere is in good agreement with reanalysis. However the NAM time

scales in the troposphere maximizes in spring instead of winter. The reanalysis show a clear maximum in winter.

When the lid is lowered and momentum is conserved, the stratospheric basic state, variability, planetary wave one structure and the blocking frequency are not significantly altered. The upward propagation of wave one is also preserved. However the downward propagation is damped such that no downward propagation time scale can be estimated. The wave one damping arises from a wave one projection of the GWD at 10 hPa, which is out-of-phase with the wave one zonal wind pattern and twice as large as in the high-lid conservative configuration. The damping is a direct result of conserving momentum and results in a more compact wave one heat flux distribution at 10 hPa as compared to the high-lid conservative configuration. The wave one heat flux histogram at 100 hPa remains in good agreement with the reanalysis. There is more wave reflection type coupling in the time-lagged NAM correlations than in the high-lid conservative configuration. The downward progression of the zonal-mean NAM anomalies takes 25 days to reach the surface, which is longer than in the high-lid conservative configuration and the reanalysis. The SSW zonal wind composite is in good agreement with both the high-lid conservative configuration and the reanalysis however, the number of SSW events decreases by a factor of 2. The seasonal cycle of the NAM time scale in the stratosphere and troposphere are reasonable however the time scales are too large. The maximum tropospheric time scale occurs in winter, which is consistent with the reanalysis.

When the lid is lowered and momentum is not conserved, the stratospheric basic state, variability, planetary wave one structure and the blocking frequency are all significantly altered. The stratospheric jet is twice as strong as when momentum is conserved and always

has significant vertical shear in the lower stratosphere. The wave one amplitude is very large in the vicinity of the model lid, particularly over the polar cap. There is also a significant decrease in the blocking frequency in the Euro-Atlantic sector and a large increase in the Pacific sector, which are consistent with the changes in the tropospheric planetary wave structure. The impact of a strong stratospheric jet and low model lid height on planetary waves and blocking had been reported by previous authors (Boville 1984, 1986; Boville and Cheng 1988). However, here it is shown that momentum conservation has a large impact, which is much larger than the model lid height. The wave propagation characteristics also change significantly when momentum is not conserved: the correlation coefficients for both the upward and downward propagating patterns increase significantly. There is much more coherent downward propagation of wave one in the low-lid non-conservative configuration than in either the low-lid or high-lid conservative configurations. The increased amount of wave reflection is confirmed by a large increase in negative wave one heat flux values at both 100 hPa and 10 hPa. The lack of wave one damping near the lid leads to a much stronger stratospheric jet and results in an increase in wave reflection off of the model lid. Finally, the stratosphere-troposphere coupling is dominated by wave reflection type coupling according to the time-lagged NAM correlations. There is no downward progression of NAM anomalies. The time scale of the zonal wind SSW event is much faster and the zonal wind remains large even after the event. Nonconservation leads to a significant decrease in the number of SSW events (by a factor of 4). The NAM time scales in both the troposphere and stratosphere are larger than in the other model configurations and the seasonal cycle in the troposphere has two maxima instead of one. Overall, the excess wave reflection in the low-lid non-conservative configuration negatively impacts the climate leading to a very strong and

more persistent stratospheric jet which is not easily perturbed and more reminiscent of the southern hemisphere jet.

Our analysis suggests the stratospheric model configuration of a climate model must conserve gravity wave momentum flux and have a high enough model lid (and vertical resolution) to properly model planetary waves and their interaction with the zonal-mean flow (both wave dissipation and wave reflection) in northern hemisphere winter. If the model lid of a climate model is placed too low then it acts as a reflecting surface for the upward propagating planetary waves. Both low-lid configurations examined here had an excess of wave reflection, which resulted in too much wave reflection type stratosphere-troposphere coupling. The coupling was improved through the act of conservation since it both reduced the strength of the mean flow and damped the planetary waves near the model lid leading to wave dissipation. In particular, when momentum was conserved in the low lid model there was a significant improvement in the seasonal cycle of the NAM time scales. The models in the IPCC AR4, which are mostly low-lid models, do not capture the observed seasonal cycle of the NAM time scales (Gerber et al. 2008a). It is possible that nonconservation and poor vertical resolution in the stratosphere contribute to the biases in the NAM time scales. (The low-lid configuration has 20 vertical levels between 300 and 10 hPa, whereas only 3 of the 13 IPCC AR4 models have more than 15 vertical levels between 300 and 10 hPa (Cordero and Forster 2006).) If the model lid of a climate model is placed high enough, above 2 hPa for instance, then it is more likely to have a better representation of planetary wave structure and propagation (as compared to a low-lid climate model) in particular with regard to wave reflection. PH03 showed that the reflecting surface in the real atmosphere develops above 10 hPa. However, there is no guarantee that the modeled

jet will develop a reflecting surface and furthermore that it will have the proper variability. The jet in the high-lid configuration examined here did develop a reflecting surface but it did not have the proper variability. A high-lid also does not guarantee the proper coupling to the troposphere: the NAM correlations and the seasonal cycle of the NAM time scale in the troposphere were biased in the high-lid conservative configuration examined here. (Note however that a high-lid does significantly reduce the errors associated with nonconservation as discussed by S09.) Many chemistry-climate models which are high-lid models also have biases in the tropospheric time scales (Gerber and coauthors 2009). Understanding how to improve models with deficiencies in wave reflection and its impact on tropospheric time scales requires a better understanding of the coupling between the mean flow and the upward and downward propagating planetary waves. The mean flow coupling to the parameterized gravity waves further complicates matters. Recent results by Harnik (2009) suggest that the time duration of the upward pulse of wave activity entering the stratosphere from the troposphere is an important factor determining whether the wave is reflected or not.

Our analysis focused on northern hemisphere winter where the observed structure and propagation characteristics of the planetary waves are well documented. In the southern hemisphere the situation is more complicated because a permanent reflecting surface develops towards late winter as part of the seasonal cycle (Harnik and Lindzen 2001). Thus, wave reflection contributes more to the coupling between the stratosphere and troposphere in that hemisphere and this may pose a challenge for the CMAM since it does not capture the reflection in the northern hemisphere. Extending the analysis to the southern hemisphere is work in progress.

Acknowledgments.

This research has been supported by the Natural Sciences and Engineering Research Council of Canada, through a Post Doctoral Fellowship to the first author. JPs contribution was funded by the NOAA Climate Program Office. The first author is grateful to Drs. Michael Sigmond and John Scinocca for performing the model simulations, to Drs. Ted Shepherd and Charles McLandress for many helpful discussions and to Dr. Mark Baldwin for providing his EOF code and to Dr. Ed Gerber for providing his code to calculate the NAM time scales. The authors are also grateful to three anonymous reviewers for helping to improve the manuscript.

REFERENCES

Andrews, D. G., J. R. Holton, and C. B. Leovy, 1987: *Middle Atmosphere Dynamics*. Academic Press, 489 pp.

Baldwin, M. P. and T. J. Dunkerton, 2001: Stratospheric harbingers of anomalous weather regimes. *Science*, **294**, 581–584.

Baldwin, M. P., D. B. Stevenson, D. D. W. Thompson, T. J. Dunkerton, A. J. Charlton, and A. O'Neill, 2003: Stratospheric memory and skill of extended-range weather forecasts. *Science*, **301**, 636–640.

Baldwin, M. P. and D. W. J. Thompson, 2009: A critical comparison of stratosphere-troposphere coupling indices. *Q. J. R. Meteorol. Soc.*, **135**, 1661–1672.

Boville, B. A., 1984: The influence of the polar night jet on the tropospheric circulation in a GCM. *J. Atmos. Sci.*, **41**, 1132–1142.

Boville, B. A., 1986: Wave-mean flow interaction in a general circulation model of the troposphere and stratosphere. *J. Atmos. Sci.*, **43**, 1711–1725.

Boville, B. A. and X. Cheng, 1988: Upper boundary effects in a general circulation model. *J. Atmos. Sci.*, **45**, 2591–2606.

Charlton, A. J. and L. M. Polvani, 2007: A new look at stratospheric sudden warmings. Part I: Climatology and modeling benchmarks. *J. Climate*, **41**, 1132–1142.

Charney, J. G. and P. G. Drazin, 1961: Propagation of planetary disturbances from the lower into the upper atmosphere. *J. Geophys. Res.*, **66**, 83–109.

Cordero, E. C. and P. M. Forster, 2006: Stratospheric variability and trends in models used for the IPCC AR4. *Atmos. Chem. Phys.*, **6**, 5369–5380.

D'Andrea, F. and coauthors, 1998: Northern Hemisphere atmospheric blocking as simulated by 15 atmospheric general circulation models in the period 1979 1988. *Climate Dyn.*, **14**, 385–407.

Eyring, V., et al., 2006: Assessment of temperature, trace species, and ozone in chemistry-climate model simulations of the recent past. *J. Geophys. Res.*, **111**, 10.1029/2006JD0073 272.

Garcia, R. and B. A. Boville, 1994: "Downward control" of the mean meridional circulation and temperature distribution of the polar winter stratosphere. *J. Atmos. Sci.*, **51**, 2238–2245.

Gerber, E. P. and coauthors, 2009: Stratosphere-troposphere coupling and annular mode variability in chemistry-climate models. *J. Geophys. Res.*, submitted.

Gerber, E. P., L. Polvani, and D. Ancukiewicz, 2008a: Annular mode time scales in the Intergovernmental Panel on Climate Change Fourth Assessment Report models. *Geophys. Res. Lett.*, **35**, doi:10.1029/2008GL035712.

Gerber, E. P., S. Voronin, and L. Polvani, 2008b: Testing the annular mode autocorrelation time scale in simple atmospheric general circulation models. *Mon. Wea. Rev.*, **136**, 1523–1536.

Harnik, N., 2009: Observed stratospheric downward reflection and its relation to upward pulses of wave activity. *J. Geophys. Res*, **114**, doi:10.1029/2008JD010493.

Harnik, N. and R. S. Lindzen, 2001: The effect of reflecting surfaces on the vertical structure and variability of stratospheric planetary waves. *J. Atmos. Sci.*, **58**, 2872–2894.

Keeley, S. P. E., R. T. Sutton, and L. C. Shaffrey, 2009: Does the north atlantic oscillation show unusual persistence on intraseasonal timescales? *Geophys. Res. Lett.*, **36**, doi:10.1029/2009GL040367.

Lau, K. M. and P. H. Chan, 1983: Short-term climate variability and atmospheric teleconnections from satellite-observed outgoing longwave radiation. Part II: Lagged correlations. *J. Atmos. Sci.*, **40**, 2751–2767.

Matsuno, T., 1970: Vertical propagation of stationary planetary waves in the winter Northern Hemisphere. *J. Atmos. Sci.*, **27**, 871–883.

McFarlane, N. A., 1987: The effect of orographically excited gravity-wave drag on the circulation of the lower stratosphere and troposphere. *J. Atmos. Sci.*, **44**, 1175–1800.

McLandress, C. and N. A. McFarlane, 1993: Interactions between orographic gravity wave drag and forced stationary planetary waves in the winter northern hemisphere middle atmosphere. *J. Atmos. Sci.*, **50**, 1966–1990.

McLandress, C. and T. G. Shepherd, 2009: Impact of climate change on stratospheric sudden warmings as simulated by the Canadian Middle Atmosphere Model. *J. Climate*, **22**, 5449–5463.

Newman, P. A., E. R. Nash, and J. E. Rosenfield, 2001: What controls the temperature in the Arctic stratosphere in the spring? *J. Geophys. Res.*, **106**, 19 999–20 010.

Perlwitz, J. and N. Harnik, 2003: Downward coupling between the stratosphere and troposphere: The relative roles of wave and zonal mean processes. *J. Climate*, **16**, 3011–3026.

Perlwitz, J. and N. Harnik, 2004: Observational evidence of a stratospheric influence on the troposphere by planetary wave reflection. *J. Climate*, **17**, 4902–4909.

Sassi, F., R. R. Garcia, D. Marsh, and K. W. Hoppel, 2010: The effect of the middle atmosphere on climate simulations of the troposphere during northern hemisphere winter: A study using low-top and high-top GCMs. *J. Atmos. Sci.*, submitted.

Shaw, T. A. and T. G. Shepherd, 2008: Raising the roof. *Nature Geosc.*, **1**, 12–13.

Shaw, T. A., M. Sigmond, T. G. Shepherd, and J. F. Scinocca, 2009: Sensitivity of simulated climate to conservation of momentum in gravity wave drag parameterization. *J. Climate*, **22**, 2726–2742.

Sigmond, M., P. J. Kushner, and J. F. Scinocca, 2008: The impact of the stratosphere on tropospheric climate change. *Geophys. Res. Lett.*, **35**, doi:10.1029/2008GL033573.

Tibaldi, S. and F. Molteni, 1990: On the operational predictability of blocking. *Tellus A*, **42**, 343–365.

List of Tables

1 The phase difference dλ °E at 65°N between the SVD wave one patterns at 500 hPa and various stratospheric levels (50, 30, 10 hPa). Negative (positive) values indicate westward (eastward) phase shifts with height and hence upward (downward) wave propagation. 35

TABLE 1. The phase difference dλ °E at 65°N between the SVD wave one patterns at 500 hPa and various stratospheric levels (50, 30, 10 hPa). Negative (positive) values indicate westward (eastward) phase shifts with height and hence upward (downward) wave propagation.

NCEP	Lag (days)	dλ °E
500 hPa; 10 hPa	-6	-135.0
500 hPa; 30 hPa	-5	-100.0
500 hPa; 50 hPa	-4	-77.5
500 hPa; 10 hPa	6	107.5
500 hPa; 30 hPa	5	80.0
500 hPa; 50 hPa	4	57.5

HIGH_C	Lag (days)	dλ °E
500 hPa; 10 hPa	-6	-123.8
500 hPa; 30 hPa	-5	-92.8
500 hPa; 50 hPa	-4	-75.9
500 hPa; 10 hPa	6	115.3
500 hPa; 30 hPa	5	90.0
500 hPa; 50 hPa	4	53.4

LOW_C	Lag (days)	dλ °E
500 hPa; 10 hPa	-6	-106.9
500 hPa; 30 hPa	-5	-84.4
500 hPa; 50 hPa	-4	-67.5
500 hPa; 10 hPa	6	101.2
500 hPa; 30 hPa	5	64.7
500 hPa; 50 hPa	4	36.6

LOW_N	Lag (days)	dλ °E
500 hPa; 10 hPa	-6	-129.4
500 hPa; 30 hPa	-5	-112.5
500 hPa; 50 hPa	-4	-98.4
500 hPa; 10 hPa	6	132.2
500 hPa; 30 hPa	5	126.6
500 hPa; 50 hPa	4	104.1

List of Figures

1 The zonal-mean zonal wind in January, February and March in the northern hemisphere for NCEP (top left), HIGH_C (top right), LOW_C (bottom left) and LOW_N (bottom right). Contour interval is 5 ms^{-1} and regions where the wind exceeds 15 ms^{-1} are shaded. Negative contours are dashed. 39

2 The vertical profile of the zonal-mean zonal wind in January, February and March averaged between 58 and 74°N (solid) and composites of years which exceed ± 0.5 standard deviations at 30 hPa (dashed) for NCEP (top left), HIGH_C (top right), LOW_C (bottom left) and LOW_N (bottom right). 40

3 The 500 hPa geopotential height field in January, February and March for HIGH_C (top left), LOW_C – HIGH_C (top right), LOW_N – HIGH_C (bottom left) and LOW_N – LOW_C (bottom right). Contour interval is 100 m (top left panel) and 25 m (remaining panels). Negative contours are dashed. Shading indicates statistically significant differences at the 95% level according to the t-test. 41

4 Blocking frequency in January, February and March for NCEP (solid), HIGH_C (dashed), LOW_C (dash-dot) and LOW_N (dotted). 42

5 The 500 hPa wave one geopotential height field in January, February and March for NCEP (top left), HIGH_C (top right), LOW_C (bottom left) and LOW_N (bottom right). Contour interval is 10 m with solid (dashed) contours indicating positive (negative) values. 43

6 Amplitude of wave one in January, February and March for NCEP (top left), HIGH_C (top right), LOW_C (bottom left) and LOW_N (bottom right). Contour interval is [25, 50, 100, 200, 400, 800] m. Shaded values indicate differences with HIGH_C which exceed 50 m. 44

7 Correlations of the temporal expansion coefficients between the leading wave one SVD mode at 500 hPa and three stratospheric levels 50 hPa (dash-dot), 30 hPa (solid) and 10 hPa (dashed) at various time lags for NCEP (top left), HIGH_C (top right), LOW_C (bottom left) and LOW_N (bottom right). 45

8 Histogram of the correlation coefficients at +6 day lag for the SVD mode between 500 hPa and 30 hPa for NCEP (top left), HIGH_C (top right), LOW_C (bottom left) and LOW_N (bottom right). 46

9 Histograms of the wave one heat flux averaged between 40 and 90°N at 100 hPa in January, February and March for NCEP (top left), HIGH_C (top right), LOW_C (bottom left) and LOW_N (bottom right). The vertical line indicates the zero value and negative values are shaded. 47

10 As in Fig. 9 but at 10 hPa. 48

11 The wave one GWD (left) and zonal wind (right) fields in January, February and March for HIGH_C (top), LOW_C (middle) and LOW_N (bottom). Contour interval is 0.01 $ms^{-1}day^{-1}$ (left) and 2 ms^{-1} (right). Negative contours are dashed. 49

12 Correlation coefficients between the NAM time series at 10 hPa and all other levels for time lags between -40 and 40 days during winter for NCEP (top left), HIGH_C (top right), LOW_C (bottom left) and LOW_N (bottom right). Contour interval is 0.1 and negative contours are dashed. Shading indicates statistically significant correlations at the 95% level. 50

13 Stratospheric sudden warming composites of zonal-mean zonal wind at 60°N and 10 hPa for NCEP (top left), HIGH_C (top right), LOW_C (bottom left) and LOW_N (bottom right). 51

14 The seasonal cycle of the NAM time scale (in days) for NCEP (top left), HIGH_C (top right), LOW_C (bottom left) and LOW_N (bottom right). Values greater than 12 days are shaded. 52

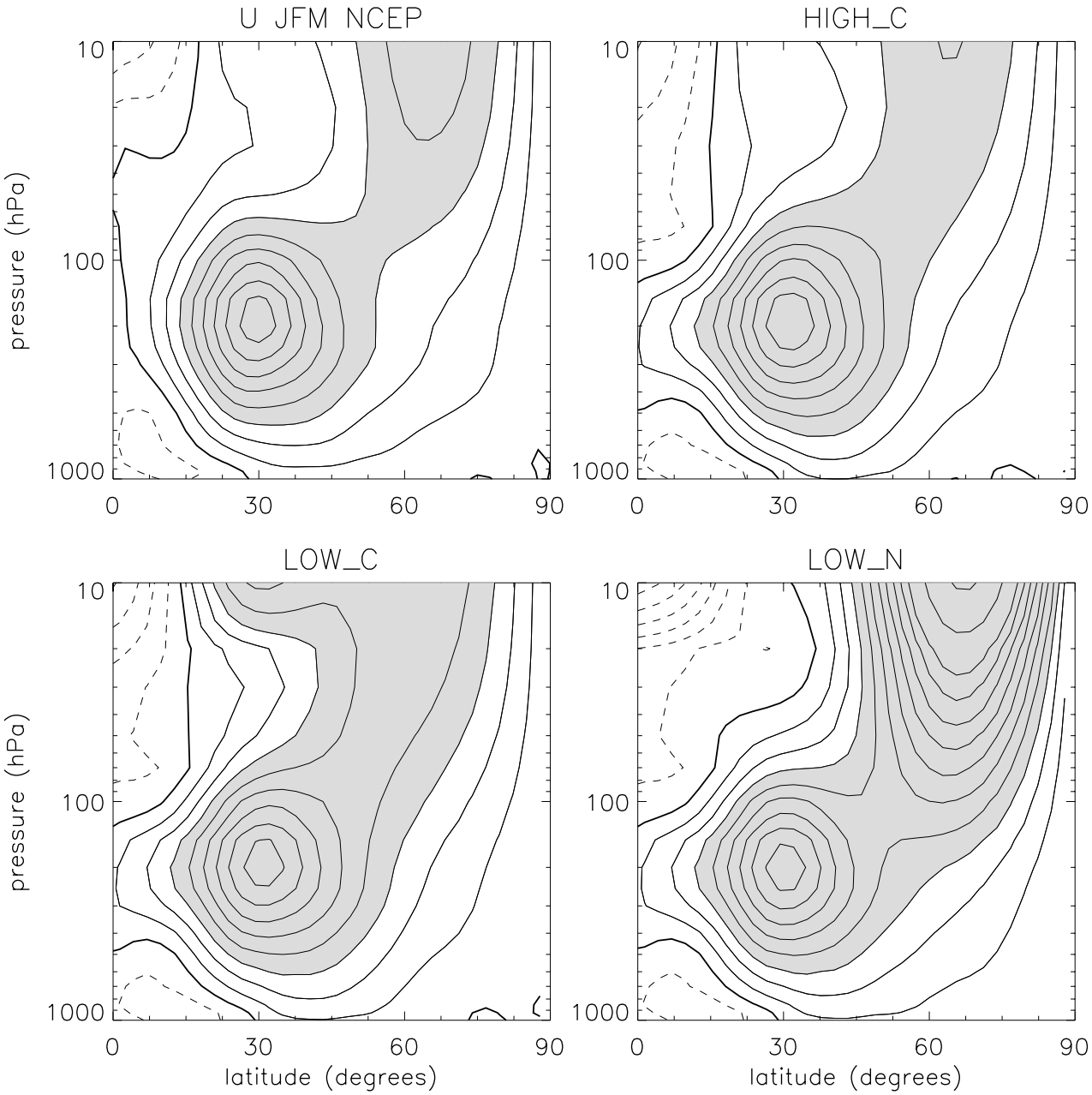

FIG. 1. The zonal-mean zonal wind in January, February and March in the northern hemisphere for NCEP (top left), HIGH_C (top right), LOW_C (bottom left) and LOW_N (bottom right). Contour interval is 5 ms^{-1} and regions where the wind exceeds 15 ms^{-1} are shaded. Negative contours are dashed.

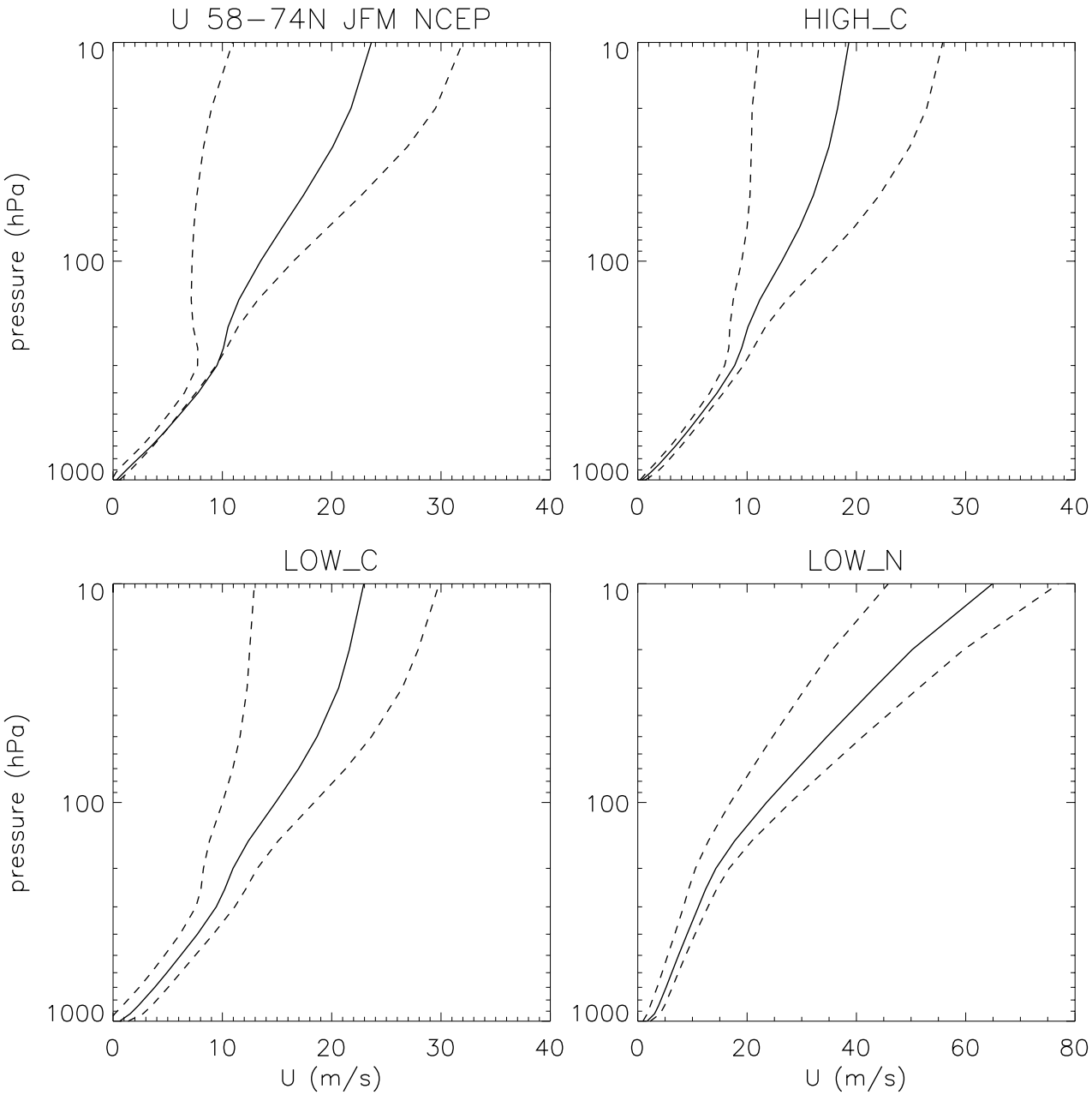

FIG. 2. The vertical profile of the zonal-mean zonal wind in January, February and March averaged between 58 and 74°N (solid) and composites of years which exceed ± 0.5 standard deviations at 30 hPa (dashed) for NCEP (top left), HIGH_C (top right), LOW_C (bottom left) and LOW_N (bottom right).

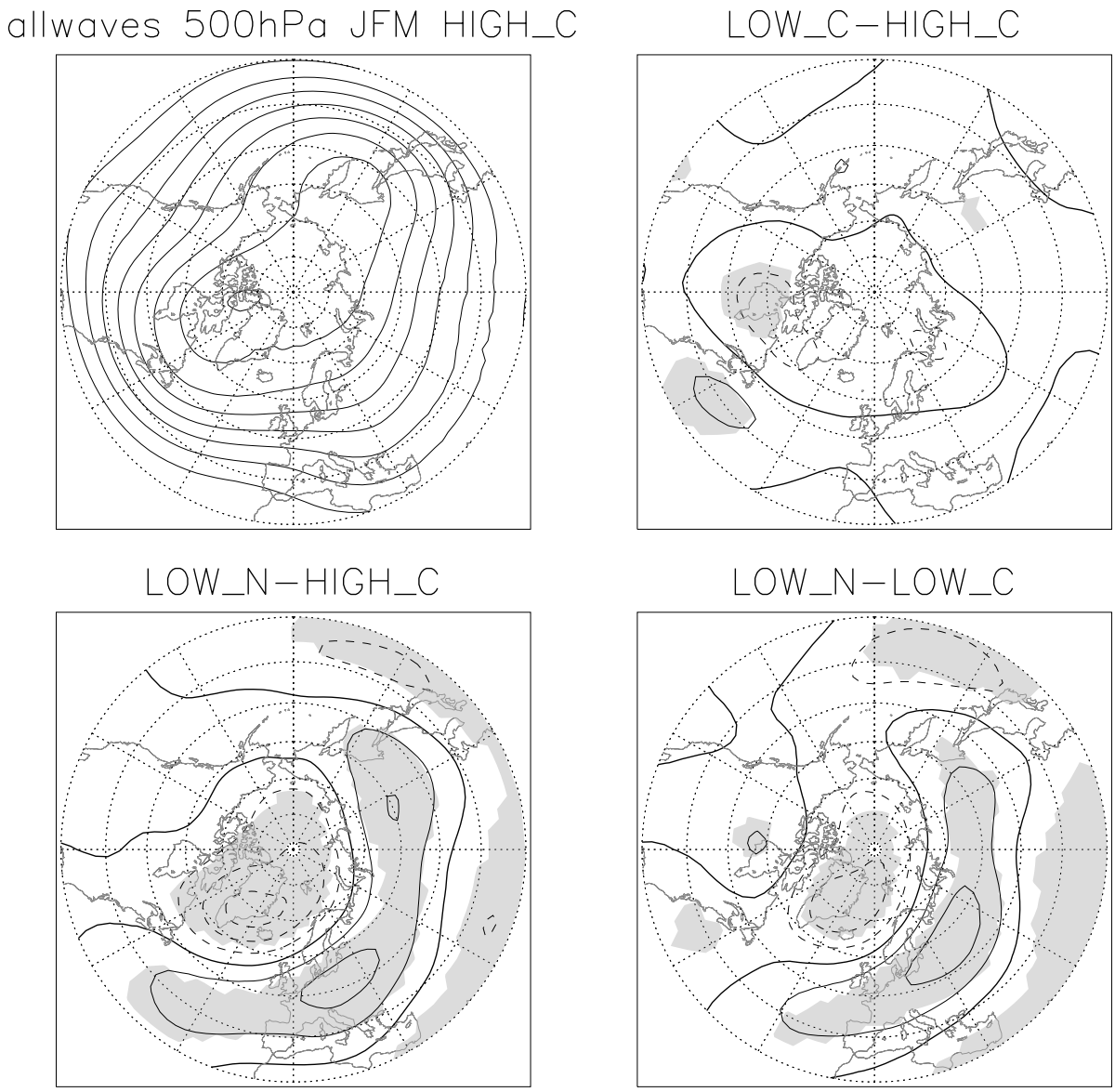

FIG. 3. The 500 hPa geopotential height field in January, February and March for HIGH_C (top left), LOW_C – HIGH_C (top right), LOW_N – HIGH_C (bottom left) and LOW_N – LOW_C (bottom right). Contour interval is 100 m (top left panel) and 25 m (remaining panels). Negative contours are dashed. Shading indicates statistically significant differences at the 95% level according to the t-test.

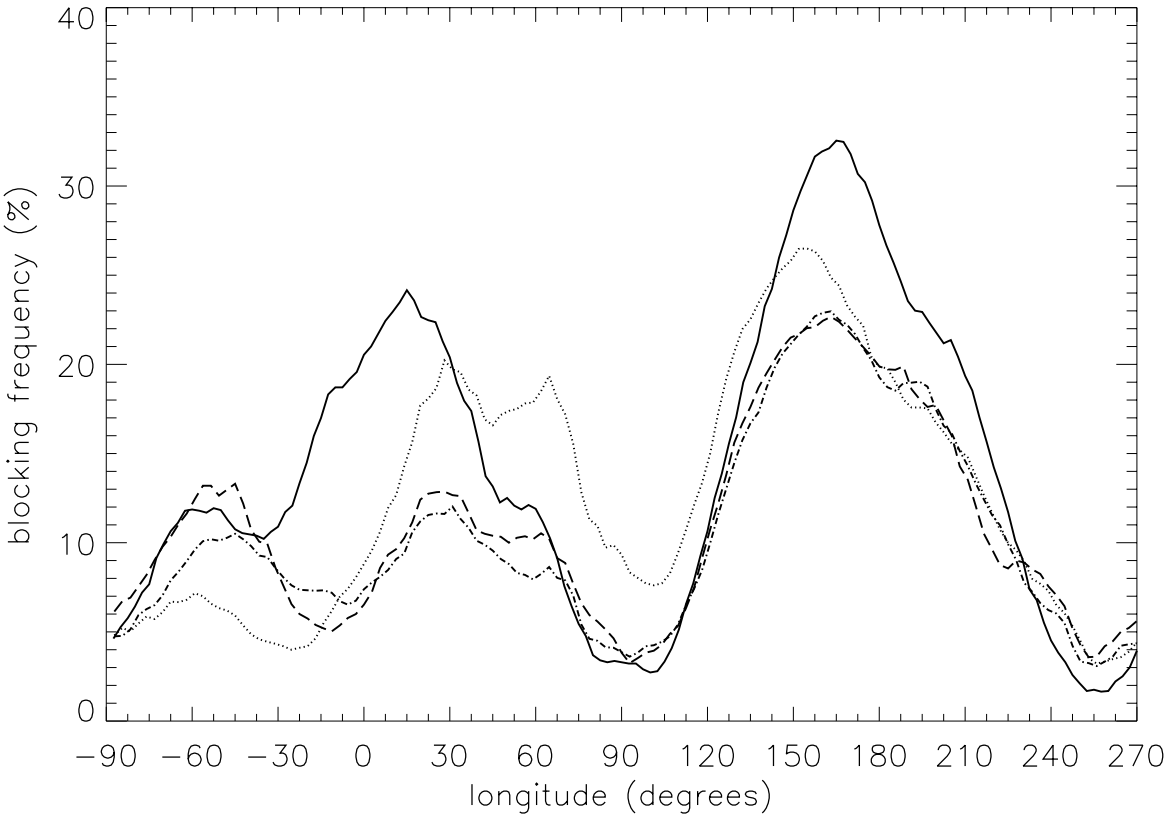

FIG. 4. Blocking frequency in January, February and March for NCEP (solid), HIGH_C (dashed), LOW_C (dash-dot) and LOW_N (dotted).

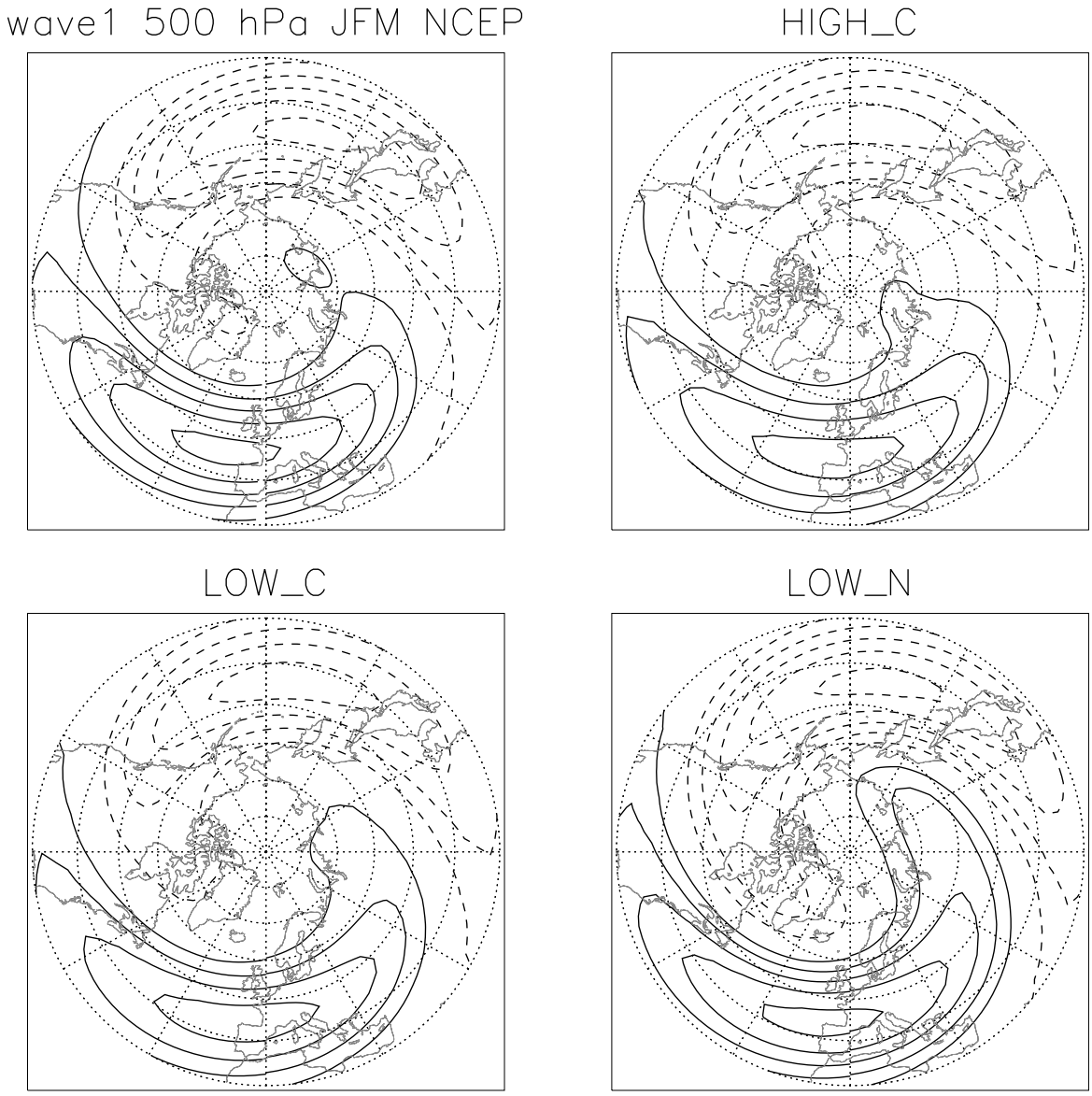

FIG. 5. The 500 hPa wave one geopotential height field in January, February and March for NCEP (top left), HIGH_C (top right), LOW_C (bottom left) and LOW_N (bottom right). Contour interval is 10 m with solid (dashed) contours indicating positive (negative) values.

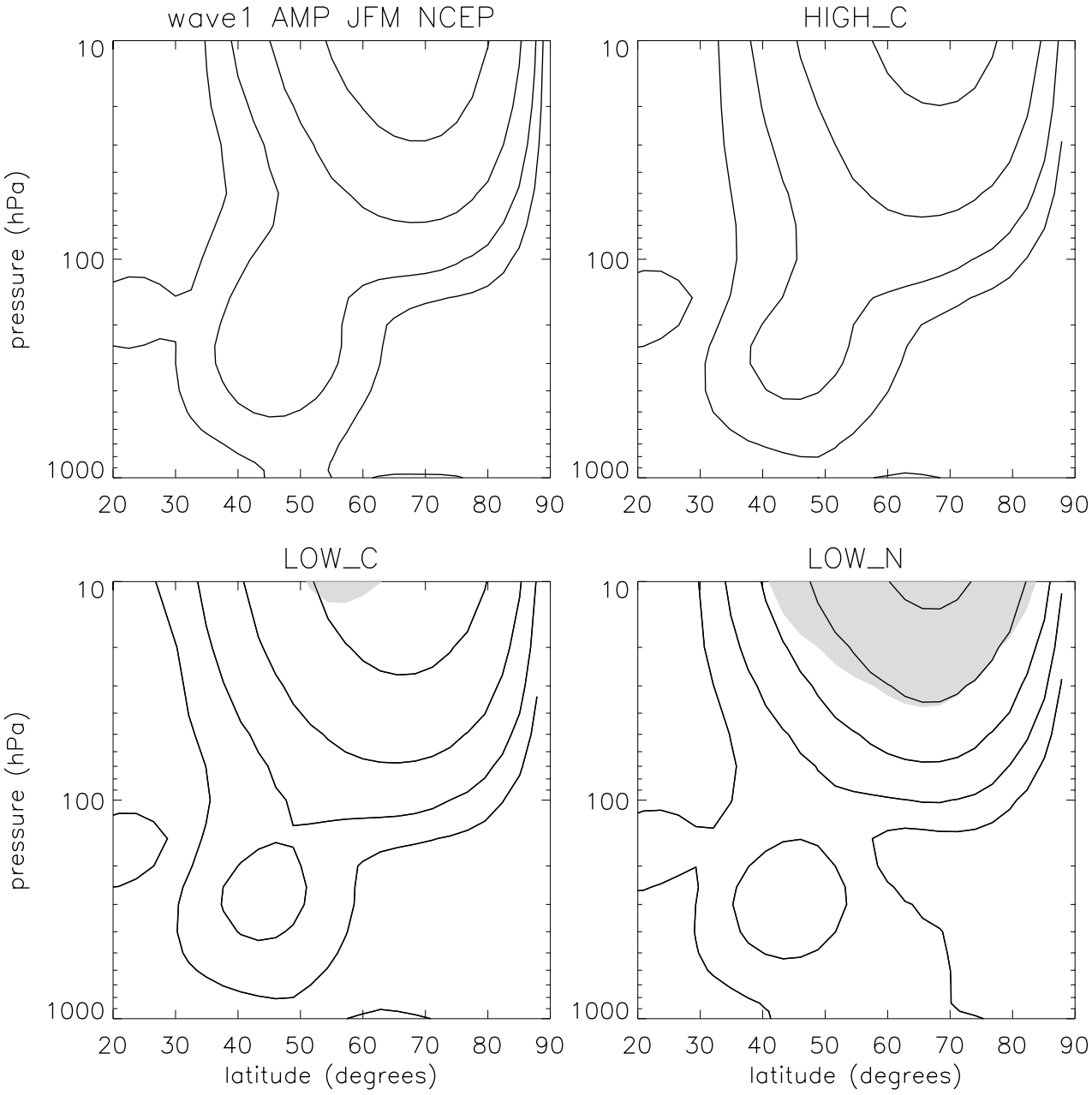

FIG. 6. Amplitude of wave one in January, February and March for NCEP (top left), HIGH_C (top right), LOW_C (bottom left) and LOW_N (bottom right). Contour interval is [25, 50, 100, 200, 400, 800] m. Shaded values indicate differences with HIGH_C which exceed 50 m.

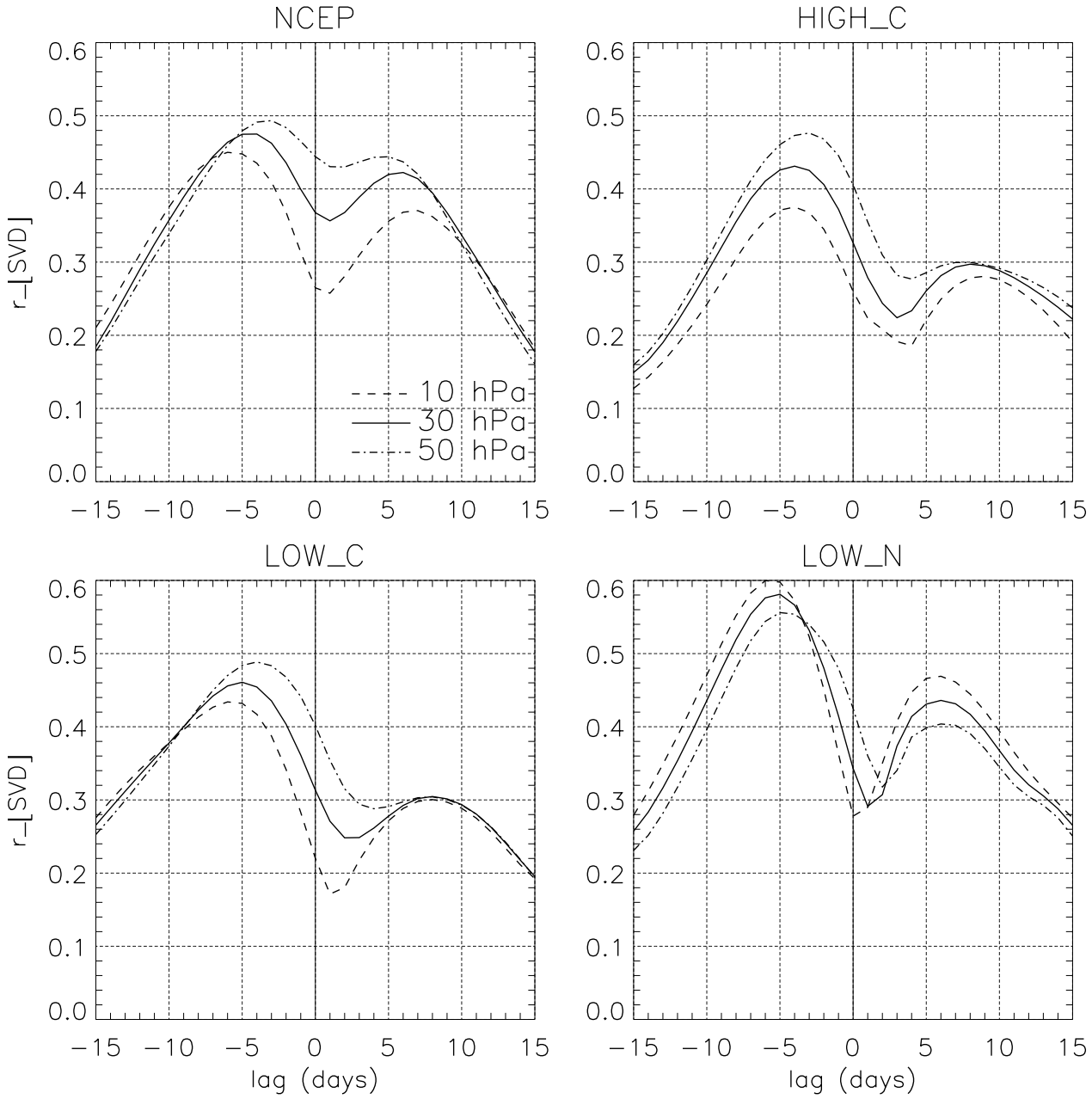

FIG. 7. Correlations of the temporal expansion coefficients between the leading wave one SVD mode at 500 hPa and three stratospheric levels 50 hPa (dash-dot), 30 hPa (solid) and 10 hPa (dashed) at various time lags for NCEP (top left), HIGH_C (top right), LOW_C (bottom left) and LOW_N (bottom right).

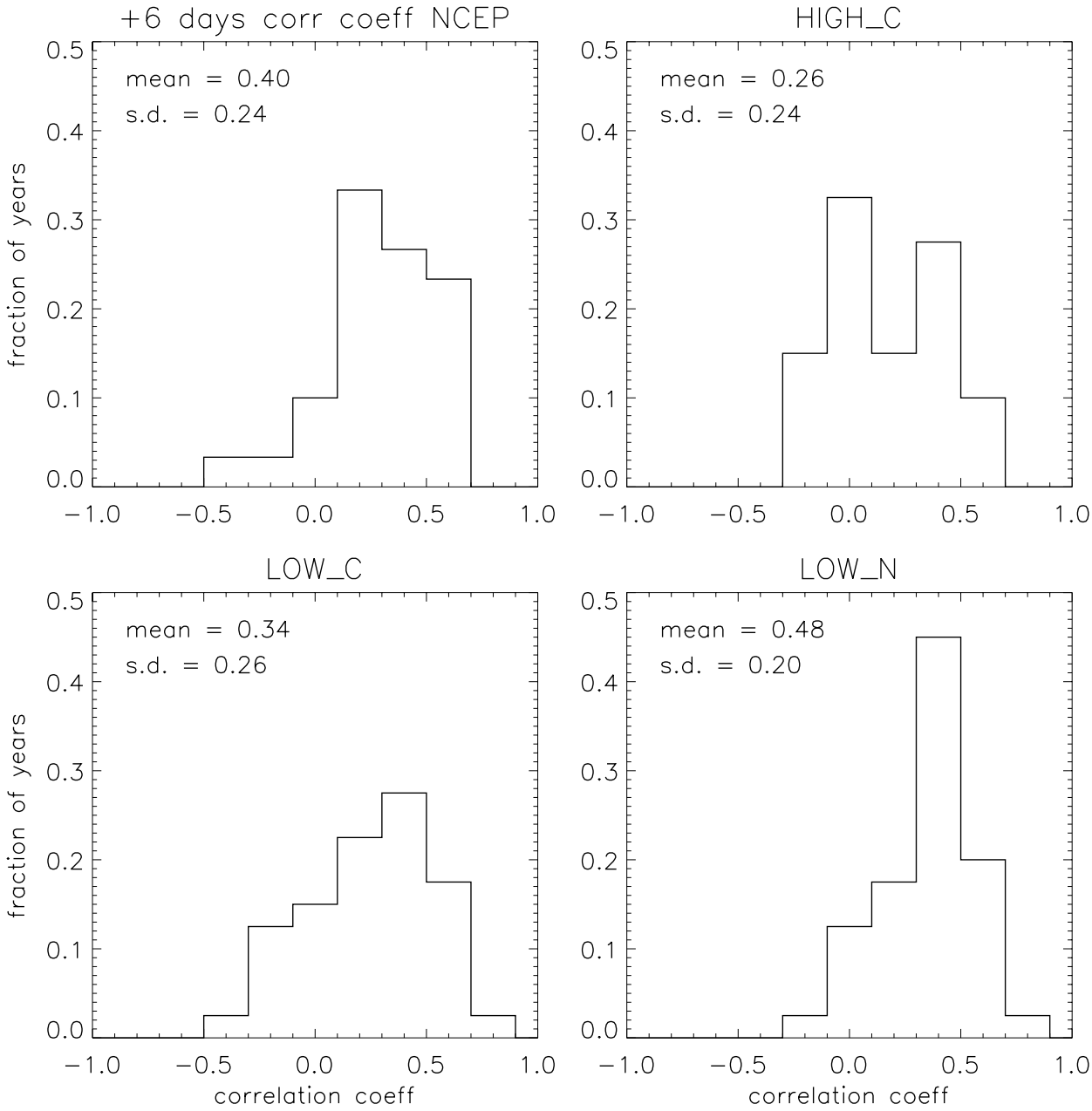

FIG. 8. Histogram of the correlation coefficients at +6 day lag for the SVD mode between 500 hPa and 30 hPa for NCEP (top left), HIGH_C (top right), LOW_C (bottom left) and LOW_N (bottom right).

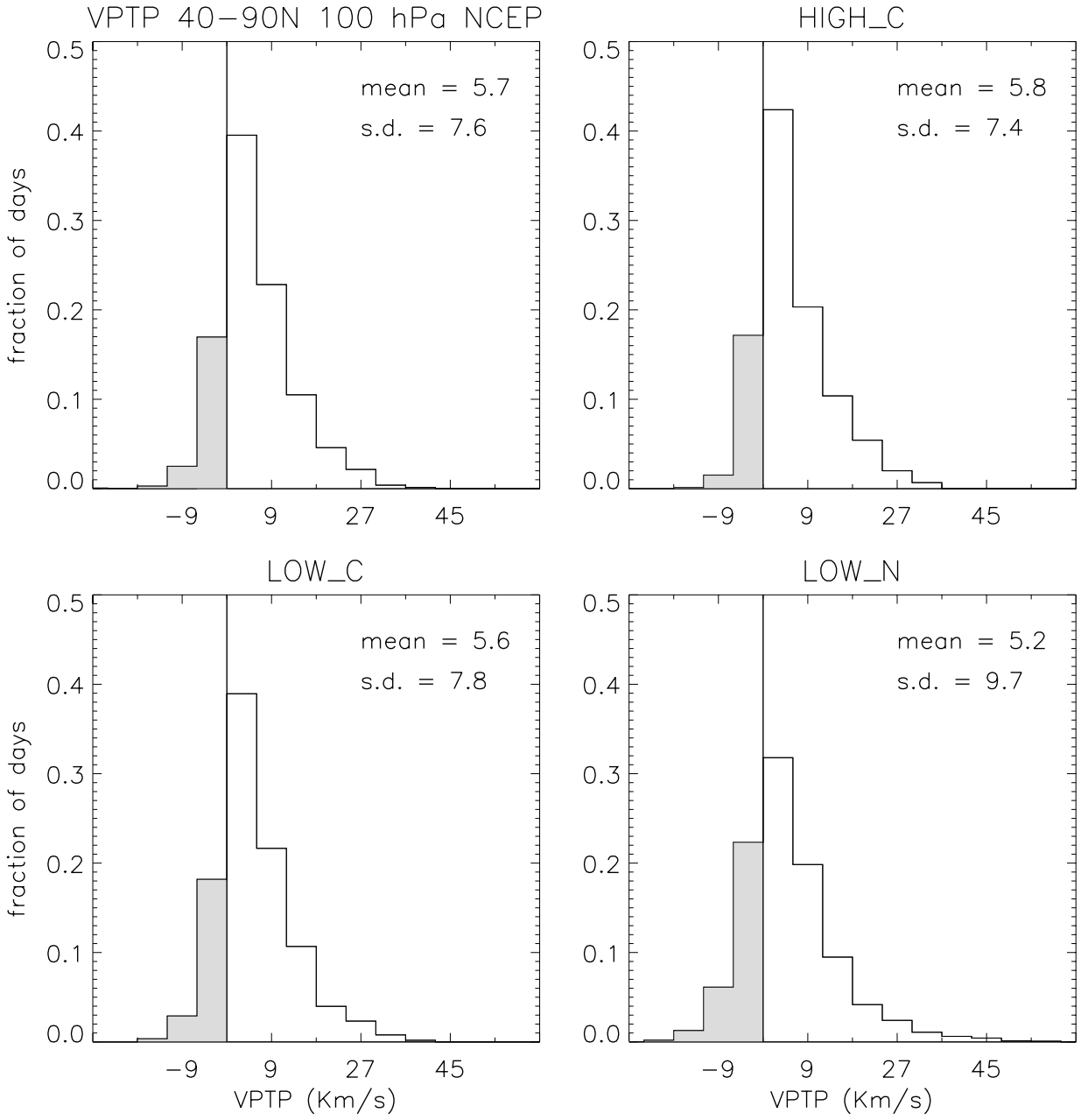

FIG. 9. Histograms of the wave one heat flux averaged between 40 and 90°N at 100 hPa in January, February and March for NCEP (top left), HIGH_C (top right), LOW_C (bottom left) and LOW_N (bottom right). The vertical line indicates the zero value and negative values are shaded.

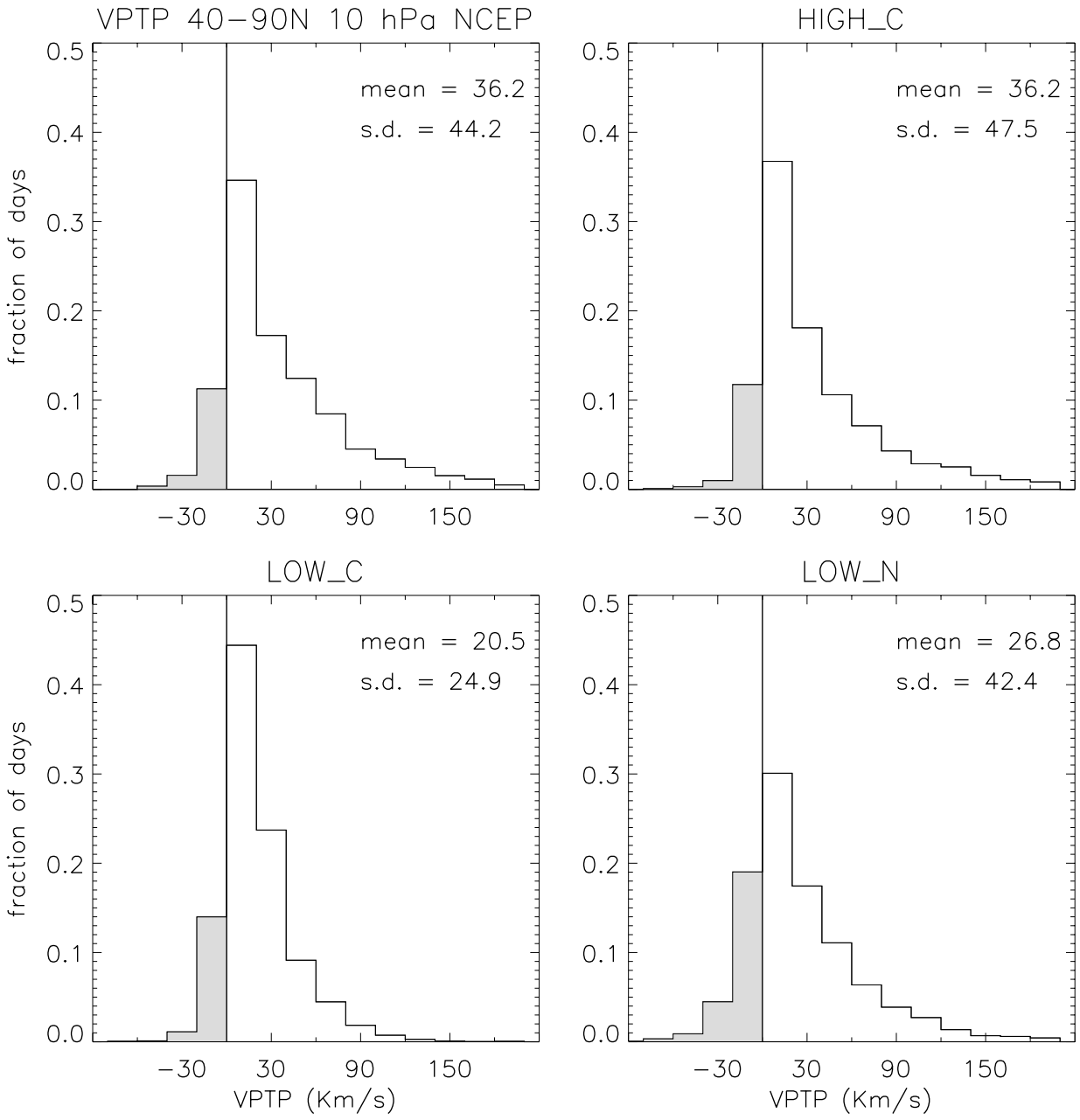

FIG. 10. As in Fig. 9 but at 10 hPa.

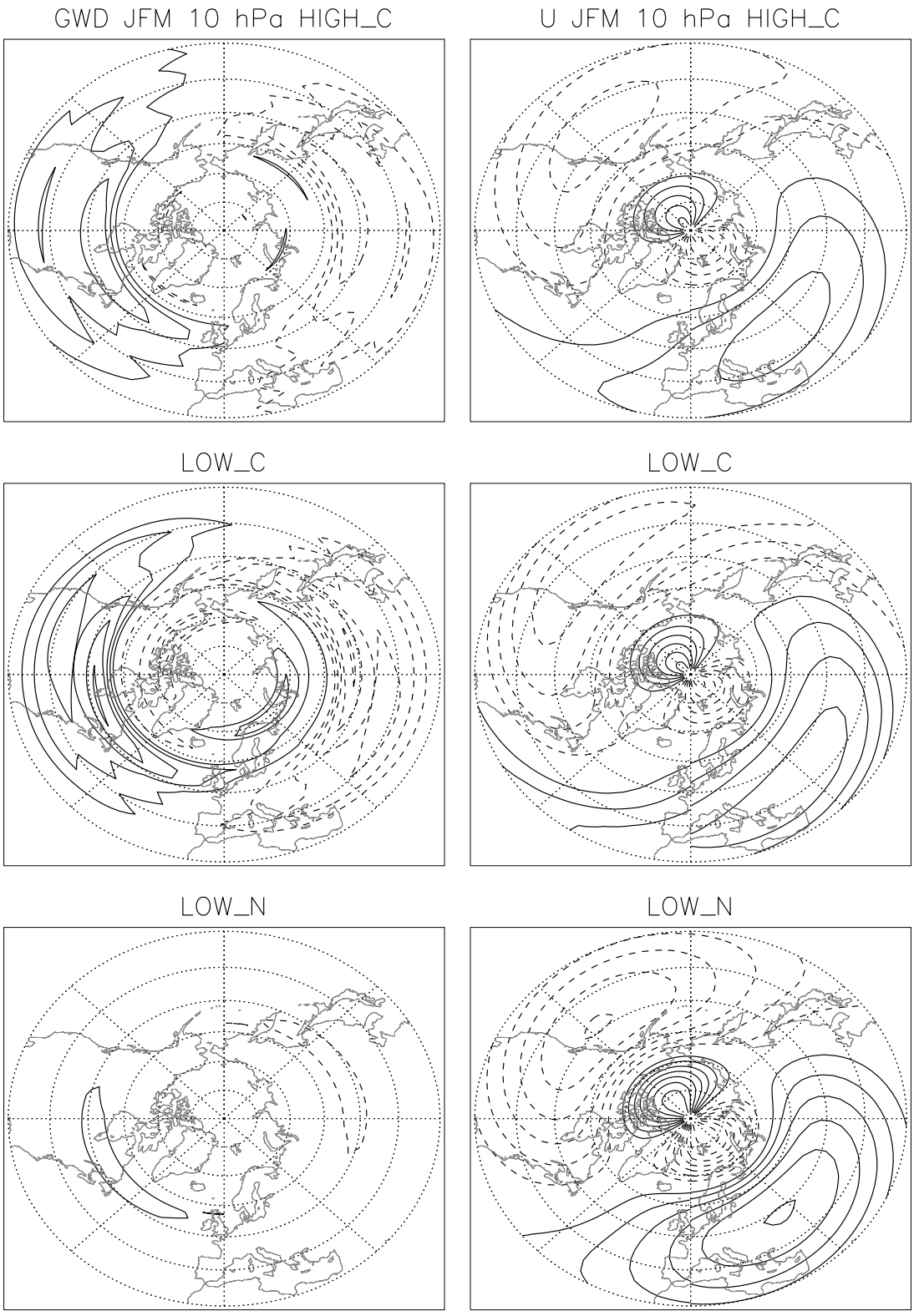

FIG. 11. The wave one GWD (left) and zonal wind (right) fields in January, February and March for HIGH_C (top), LOW_C (middle) and LOW_N (bottom). Contour interval is 0.01 $ms^{-1}day^{-1}$ (left) and 2 ms^{-1} (right). Negative contours are dashed.

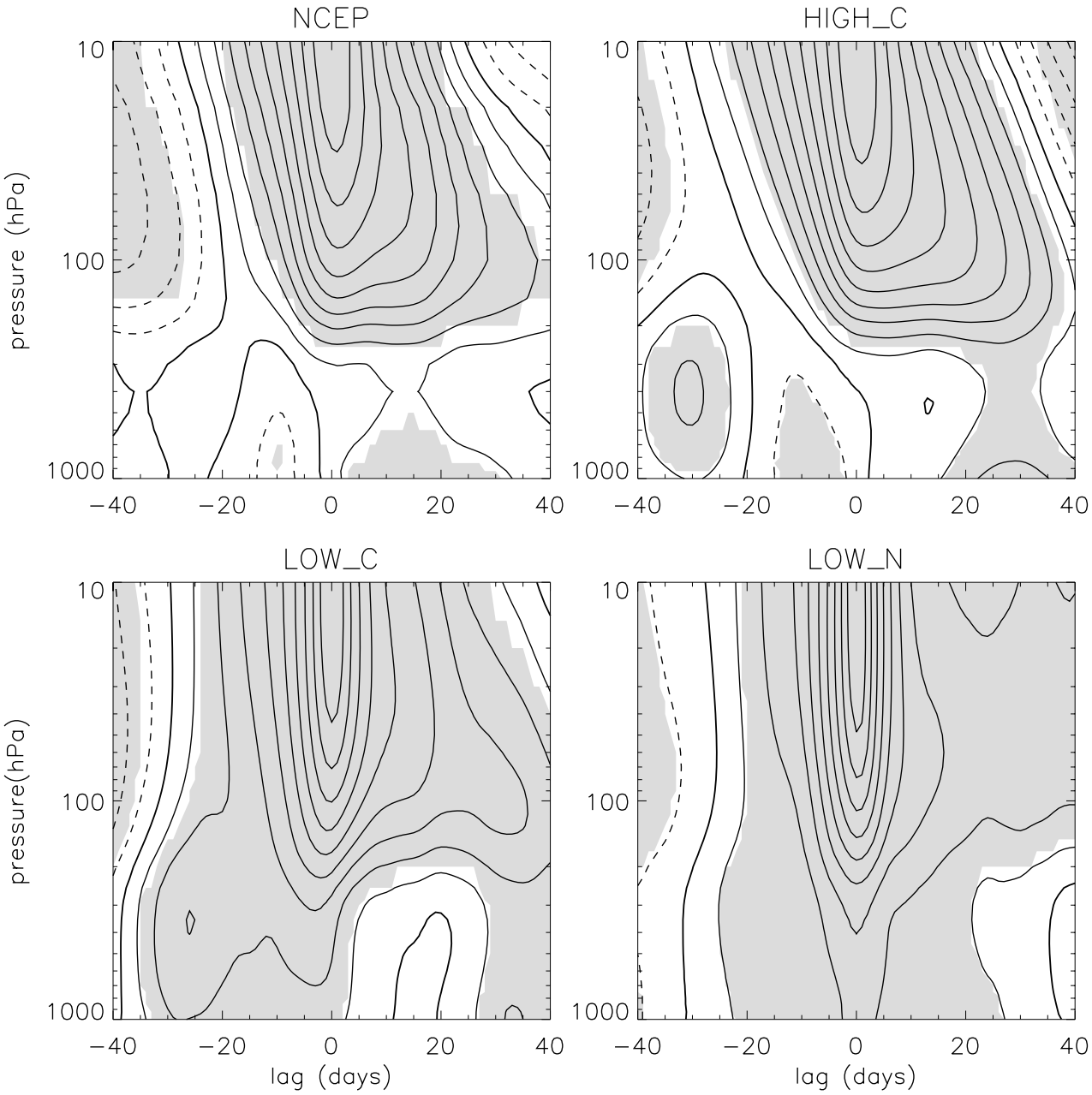

FIG. 12. Correlation coefficients between the NAM time series at 10 hPa and all other levels for time lags between -40 and 40 days during winter for NCEP (top left), HIGH_C (top right), LOW_C (bottom left) and LOW_N (bottom right). Contour interval is 0.1 and negative contours are dashed. Shading indicates statistically significant correlations at the 95% level.

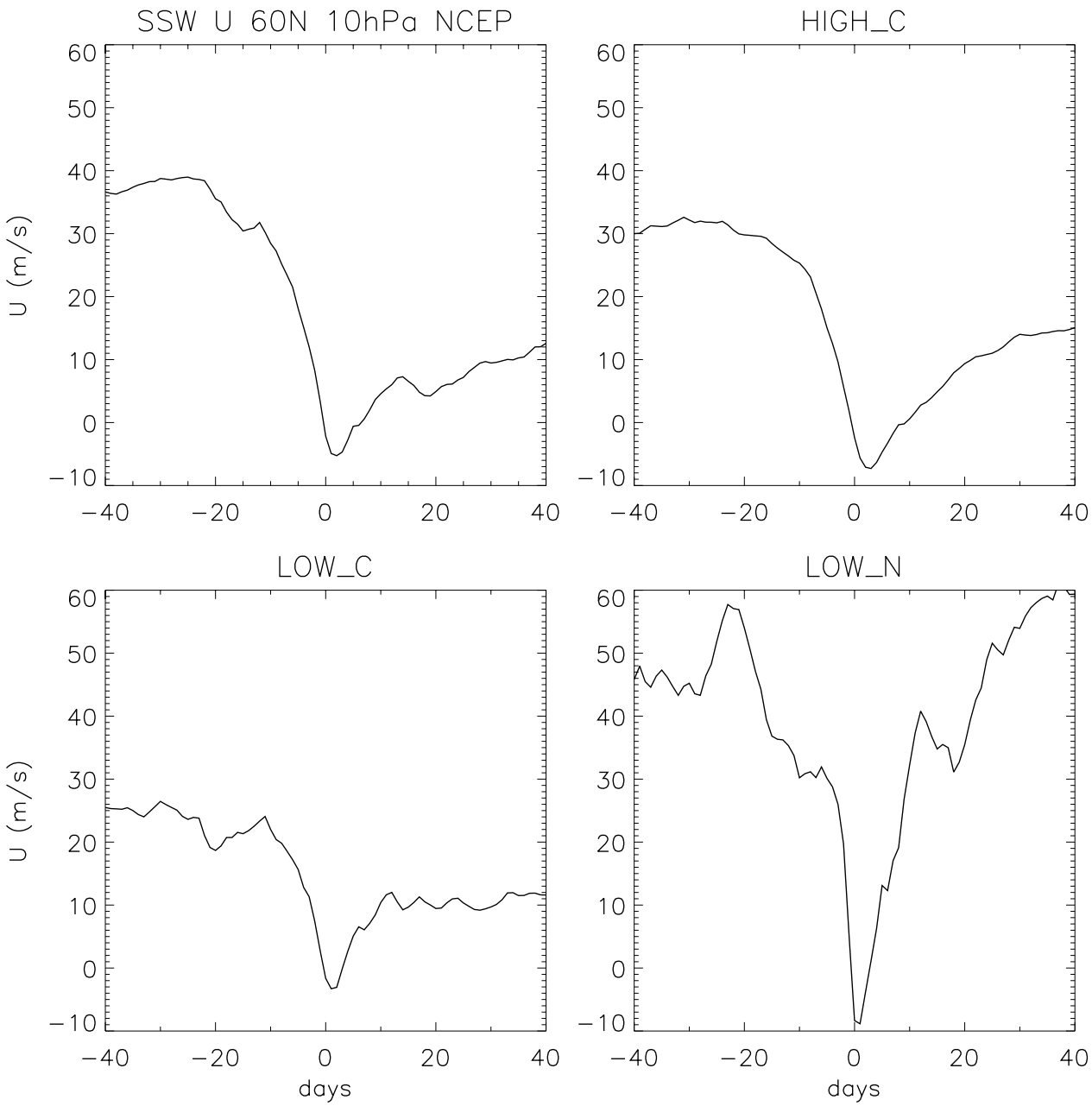

FIG. 13. Stratospheric sudden warming composites of zonal-mean zonal wind at 60°N and 10 hPa for NCEP (top left), HIGH_C (top right), LOW_C (bottom left) and LOW_N (bottom right).

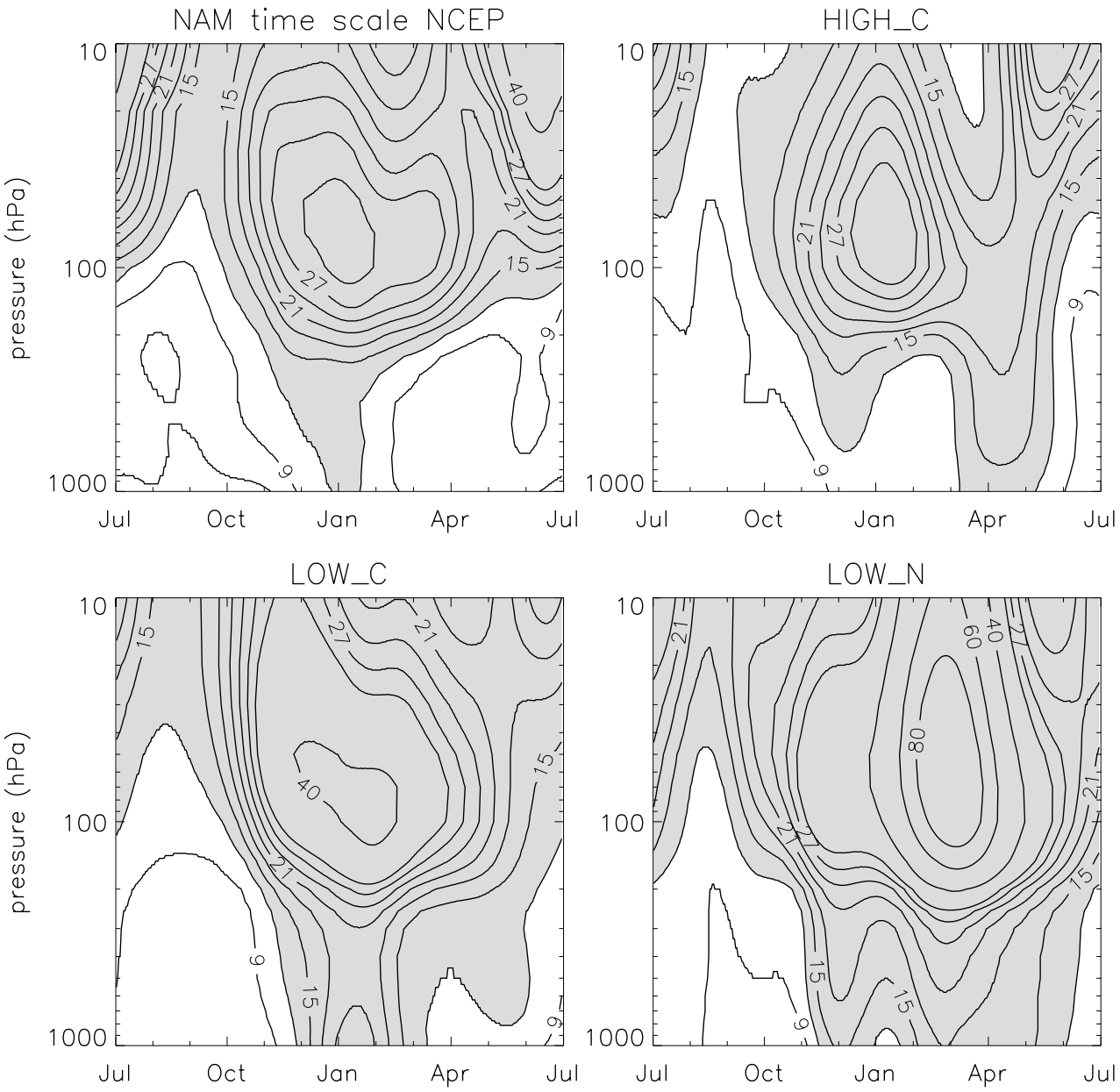

FIG. 14. The seasonal cycle of the NAM time scale (in days) for NCEP (top left), HIGH_C (top right), LOW_C (bottom left) and LOW_N (bottom right). Values greater than 12 days are shaded.